SEMI-ANNUAL REPORT

FOR

NASA GRANT NAG-1-1063

PERIOD: FEBRUARY 1, 1991 - JULY 1 1991

PRINCIPAL INVESTIGATOR:

BARRY T. SMITH

APPLIED SCIENCE PROGRAM
COLLEGE OF WILLIAM AND MARY
WILLIAMSBURG, VA 23185

NASA TECHNICAL OFFICER:

DR. PATRICK H. JOHNSTON

NONDESTRUCTIVE EVALUATION SCIENCES BRANCH
NASA, LANGLEY RESEARCH CENTER
MAIL STOP 231
HAMPTON, VA 23665

The first half of this grant period was focused on investigating impact generated delaminations in two class of composite materials. The first set of materials were woven composites with through the thickness reinforcements, and the second set was an investigation of impact damage modes in thermoset and thermoplastic composites. This work resulted in two publications. The manuscripts for both are included here. The first article " Characterization of Damage Modes in Impacted Thermoset and Thermoplastic Composites", K.Srinivasan, W.C. Jackson, B.T. Smith, and J.A. Hinkley, has been accepted to the Journal of Reinforced Plastics and Composites. The second publication, "Compression Response of Thick Layer Composite Laminates with Through-the Thickness Reinforcement", Gary L. Farley, Barry T. Smith and Janice Maiden, has been submitted to Journal of Reinforced Plastics and Composites.

Characterization of Damage Modes in Impacted Thermoset and Thermoplastic Composites

K. SRINIVASAN

Department of Mechanical Engineering and Mechanics

Old Dominion University

Norfolk, VA 23529

W. C. JACKSON

US Army Aerostructures Directorate (AVSCOM)

NASA Langley Research Center

Hampton, VA 23665

B. T. SMITH

Applied Sciences

College of William and Mary

Williamsburg, VA 23185

AND J. A. HINKLEY

Materials Division

NASA Langley Research Center

Hampton, VA 23665

ABSTRACT: Composite materials remain extremely vulnerable to out-of-plane impact loads, which may lead to severe losses in strength and stiffness. Impact induced damage is often a complex mixture of transverse cracks, delaminations and fiber failures. An experimental investigation was undertaken to quantify damage tolerance and resistance in composite materials impacted using the drop-weight method. Tests were conducted on laminates of several different carbon-fiber composite systems such as epoxies, modified epoxies, and amorphous and semicrystalline thermoplastics. In this paper, impacted composite specimens have been examined using destructive and non-destructive techniques to establish the characteristic damage states. Specifically, optical microscopy, ultrasonic and scanning electron microscopy techniques have been used to identify impact induced damage mechanisms. Damage propagation during post impact compression was also studied.

INTRODUCTION

Composite materials made of continuous carbon fibers and high performance polymers are gaining increasing acceptance in aerospace structures due to potential weight savings and efficient design considerations. These materials are being considered for primary (load bearing) structural applications in commercial and military aircraft. An important design consideration is low velocity impact by foreign objects (*e.g.* bird hits, runway debris, tool drop, hail *etc*). As the first generation of epoxy based composites was extremely susceptible to impact damage (with attendant mechanical property losses), newer damage tolerant and damage resistant resins have been synthesized for composite applications. Laminated composites are known to undergo severe internal damage resulting from impact events that may or may not be evident from a surface inspection. Further, surface damage often offers an

inadequate description of the complete damage state that exists within the laminate. Typical damage zones in impacted laminates consist of transverse matrix cracks, delaminations, fiber failures and combinations of these. Impact damage in composites may result in a severe loss in load bearing capacity, particularly with respect to post-impact compression.

In a previous study [1, 2], a newly developed impact fixture was used to establish impact and compression after impact data on several composite systems. The goal of that study was to evaluate the impact damage resistance and residual compressive strength of various composite systems and to determine the effect of material characteristics on impact damage tolerance. Several composite systems reflecting generic categories of resin behavior (such as brittle thermosets, toughened thermosets and amorphous and semicrystalline thermoplastics) were selected for this study. These materials possess widely different chemistries, cure/consolidation mechanisms, morphologies/microstructures and deformational capabilities. The present study focuses on mapping the resulting impact and post impact compressive damage patterns in samples used in that study. The mapping was done with a view towards reconstructing the characteristic damage due to the impact event and eliciting key details of the damage mechanisms. Conventional fractographic techniques (optical microscopy and SEM) have been supplemented with novel ultrasonic techniques to achieve this characterization. This information, in conjunction with the mechanical data [1, 2] provides comprehensive information on the response of composite laminates to impact.

EXPERIMENTAL PROCEDURE

Materials

The materials selected for evaluation are outlined in Table I. Also included in the table are typical fiber volume fractions of the laminates made for this study.

TABLE I

MATERIAL	NATURE	SUPPLIER	V_f
3501-6/AS-4	Epoxy	Hercules	59.5
977-2/IM-7	Modified Epoxy	ICI	61.0
T3900-2/T800-H	Modified Epoxy	Hexcel	58.4
PEEK/AS-4	Semicrystalline Thermoplastic	ICI	63.0
PEEK/IM-7	Semicrystalline Thermoplastic	ICI	62.9
ULTEM1000/AS-4	Amorphous Polyimide	In House	56.8

The first material was used as a baseline material since it is in wide commercial use and represents a highly crosslinked brittle epoxy. The 977-2 and T3900-2 materials represent various approaches to toughening thermosets; one being a co-continous network (977-2), while the other is a bi-phase system. The last three materials represent thermoplastic polymer matrix composites; PEEK being semicrystalline and Ultem representing an amorphous polyimide. The PEEK material was available with two types of reinforcing fibers: AS-4 and the newer IM-7.

Specimens

All materials were processed in house according to manufacturer specifications. Quasi-isotropic laminates were made in two thicknesses (24 and 48 plies thick) with a layup designation of $(-45/0/45/90)_{ns}$ (n = 3 or 6). Typical laminate fiber volume fractions are given in Table I. Specimens, 12.1 X 10.2 cm, were then cut from these plates with the 0-degree direction along the longer specimen direction. Typical thicknesses ranged from 0.312 to 0.371 cm for the 24 ply and from 0.648 to 0.721 cm for the 48 ply samples. All sample edges were ground to ensure flat and perpendicular faces. Routine C-Scans were performed to ensure that samples were free of gross defects prior to the impact test.

Experimental Details

The fixture (Fig. 1) consisted of a pair of 15 cm square picture frame blocks, made of mild steel, each 1.91 cm thick and having a central 7.62 X 7.62 cm cutout. The sample was clamped between the two blocks by ten bolts. The sample was aligned so as to be impacted at the center of the plate.

An instrumented drop-weight impacter (Fig. 2) consisted of a 2.74-kg striker with a 1.27-cm-diameter stainless steel hemispherical tup. Impact and rebound velocities were measured with a laser and a photoelectric detector. The striker was instrumented to measure both load (via a strain gage assembly) and acceleration. The incident impact energy on the specimen was changed by varying the drop height of the striker in the guide tube. At least six different heights were employed for each material. Typical impact energies ranged from 500 to 9000 J/m. After impact, the specimens were C-Scanned to determine damage profiles. Some samples were photographed to preserve a record of the surface damage. Certain samples were sectioned, polished and viewed through a low magnification optical microscope to

view the damage patterns due to the impact. A large majority of the samples were subjected to plate compression in an edge supported compression fixture. This procedure was used to establish CAI strengths and strains. Selected post impact compression samples were also sectioned, polished and photographed using a low magnification microscope. All microscopic specimens were polished in accordance with standard metallographic techniques.

In addition to optical microscopic observations, some impacted laminates were examined using a Scanning Electron Microscope. Gold coated samples taken from around the impacted area were viewed with magnifications up to 1000X to determine mechanisms of impact induced damage.

C-Scan techniques though convenient and useful, fail to provide information on through the depth damage accumulation. The lack of detailed impact damage information has often been supplanted by empirical correlations, such as relationships between impact damage and open holes or implanted delaminations [3]. While such techniques are useful, a fundamental knowledge of the impact damage details is still needed. Hence, a recently developed ultrasonic technique [4] has been used to determine internal damage states. Briefly, the ultrasonic evaluation was performed in a water bath using a 5 MHz transducer with a 0.318 cm aperture and a 5.08 cm focal point. The transducer was operated in a pulse - echo mode and was excited by a square wave pulser. The return signal was amplified and fed to a Time Gain Compensated (TGC) amplifier. A digitizer with a sampling rate of 100 MHz and nominal 8 bit dynamic range acquired the signal and passed it to the computer for later analysis. The entire ultrasonic wave was digitized to include front, back and interior surface reflections. A spatial sampling rate of 1 mm was on the order of a 3dB point spread for the transducer as determined experimentally. A typical sampling size was 8 X 8 cm. The TGC had a 50 MHz bandwidth, a 50 dB gain and a control bandwidth of 5

MHz. In order to enhance the effective dynamic range, the front surface signal was attenuated and the interior and back surface signals were enhanced to the input limit of the digitizer. The data was post - processed using a Fourier deconvolution and analytic magnitude signal processing techniques to provide volumetric views of the sample at any depth. A discussion of this technique has been presented previously [4]. Processed waveforms were assembled into a three dimensional array in position (x - y) and time. Progressive slices in time yielded a movie in which each frame (equivalent to a digitizer channel time) gave a view deeper in the sample. The signal sources at the same depth were in phase and the larger amplitude backscattered signal corresponded to an impact generated delamination. Individual time slices could also be stored and printed to yield a hard copy of the ply level damage patterns.

RESULTS AND DISCUSSION

Figure 3 depicts a planar measure of the extent of delamination (determined by C - Scans) in the composite samples as a function of the incident impact energy on the plate. Though it discounts delaminated areas that lie on top of one another, it is still instructive from a materials classification viewpoint. For identical energies of impact, the 3501-6/AS-4 material shows the greatest damage while the Ultem 1000/AS-4 material shows the least. This is important while considering the relative damage resistances of the different materials. Further, the slope of the curve fitted line for each of the materials (except T3900-2/T800-H and Ultem 1000/AS-4) increases continuously with impact energy (*i.e.*, the rate of damage creation increases with the incident impact energy). Also, the divergences in the C-Scan areas among these materials is most significant at the higher impact energies. The differences between the PEEK/IM-7 and PEEK/AS-4 materials appears negligible, implying that the damage resistance to impact is a strong function of the matrix material.

A few impacted specimens from each material system were sectioned and polished to determine the characteristic damage state. When viewed through an optical microscope at low magnifications, all materials showed a characteristic cone of damage, the size of which depended on the level of incident impact energy and the specific material involved. This cone of damage, comprised of transverse matrix cracks and delaminations, had its apex at the top (near the impact surface), and a widening base through the thickness of the laminate. This is shown schematically in Fig. 4. The 3501-6/AS-4 epoxy material was the most damage prone, with numerous transverse cracks and delaminations at nearly every interface. For comparable C-Scan projected damage areas, both PEEK/AS-4 and PEEK/IM-7 showed fewer transverse cracks and delaminations than the epoxy material, further, these were more concentrated on the tensile side (*i.e.* the bottom half of the impacted panel's thickness). The 977-2/IM-7 material showed similar damage characteristics. The 3900-2/T800-H material (Fig. 5) showed excessive matrix cracking in a very small localized cone of damage directly under the impact site. Damage in the Ultem material was similarly contained in a very small region under the impacting tup (Fig. 6), however the damage was mostly confined to the tensile side of the plate. Both these observations are consistent with the results of Fig. 3 which show the T3900-2 and Ultem materials to be most resistant to impact damage.

In the SEM, sufficiently far removed from the immediate impact area, most of the material systems showed characteristic hackle marks, commonly seen in samples tested under conditions leading to shear delamination [6]. In these, the resin between the fibers failed in a series of parallel cracks which were transverse to the fibers and inclined at an angle to the interlaminar plane (Fig. 7). Also evident in Fig. 7 is a matrix crack that acts as a bridge between delaminations on sequential interfaces. The 977-2/IM-7 and epoxy material showed some evidence of bare fibers (Fig. 8). Within the

impact area, the Ultem 1000 material showed extensive deformation, indicating the tortuous nature of the crack path (Fig. 9). The T3900-2/T800-H material likewise showed considerable fragmentation. Only the PEEK and Ultem samples did not form hackle marks. Both PEEK/IM-7 and PEEK/AS-4 were characterized by excellent fiber-matrix adhesion (Fig. 10).

One representative sample of each material that was subject to plate compression was sectioned along the loading axis, polished, and viewed using low magnification microscopy. Delamination growth was detected by visually comparing the C-Scans before compression to the compressively failed specimens. Several different types of failure modes were observed. For example, in the 977-2/IM-7 material (Figs. 11 and 12), the compression caused extensive internal delamination growth (to the edge of the sample) leading to the formation of several sublaminates. The microbuckling of these delamination-induced sublaminates led to final failure. The PEEK/AS-4 material failure is characterized by fewer delaminations and numerous transverse cracks (Fig. 13). Here, the delaminations appeared to be induced by a concerted transverse shear band deformation of several plies (typically bounded by 0° plies). This type of behavior was also exhibited by other material systems and is detailed later. The PEEK/IM-7 sample showed some delamination growth, numerous transverse cracks and several subsurface microbuckle bands. The U1000/AS-4 material (Fig. 14) showed little delamination growth, but a broad central shear band served as a site for ultimate microbuckling failure. Though the T3900-2/T800-H sample had some delamination growth, the narrow zone of extensive impact induced damage showed numerous fiber failures and cracks (Fig. 15). The 3501-6/AS-4 showed extensive delamination and microbuckling.

Several laminates were subjected to the through-the-thickness ultrasonic technique outlined earlier. The typical ply-by-ply damage state of an impacted

laminate is displayed in Fig. 16. The numbers represent the interfaces between plies of different orientations starting from the top of the laminate. The lighter regions in the figure indicate areas that are delaminated. In any ply, the damage state consists of wedge shaped delaminations bounded between the fiber orientations of the plies above and below the lamina interface. From the central impacted point, these wedge shaped delaminations spiral continually throughout the thickness of the panel to create sublaminates that maintain structural and mechanical continuity. This characteristic damage state is seen in laminates impacted at both high and low energy levels. Dost *et al* [5] have postulated that these wedge shaped delaminations are linked by transverse matrix cracks in plies adjacent to each delamination, a finding that is confirmed by the evidence in Figs. 7 and 16.

In considering the ultrasonic and microscopic evidence, the picture that emerges is one in which the impact produced transverse matrix cracks and delaminations at several ply interfaces. The sublaminates formed maintain complex spatial, structural and mechanical continuity. When subject to post-impact compression, these laminates show two types of damage propagation as shown schematically in Fig. 17.

Sublaminates formed by impact induced delaminations have a reduced bending stiffness compared to the undamaged laminate. As the compressive load exceeded a critical value, localized outerply buckling was one of the first events of failure. This was visually witnessed by watching moire fringe patterns develop in the impacted region indicating localized out-of-plane deformations. Compressive damage growth in impacted specimens occurred differently in different materials. The 977-2 and epoxy materials showed extensive delamination growth causing the laminate to split into several longitudinal sublaminates. Final failure occurred when one or more of these sublaminates failed by buckling due to reduced lateral support. In the PEEK and Ultem materials, final failure was also triggered by delamination induced sublaminate

buckling. But in these materials, delaminations appeared to be induced by concerted shear deformation of a few plies typically bounded by 0° plies. Sheared failures of the 0° plies were frequently seen in these samples.

CONCLUSIONS

An experimental study was undertaken to identify the failure mechanisms in composite laminates due to impacts and to understand damage propagation in post-impact compression.

Visible evidence of impact damage was often minor compared to the internal damage suffered due to the impact. This internal damage typically consisted of matrix cracks and delaminations. Fiber failures were not pronounced in the range of impact energies studied. Optical microscopic examinations of the impacted laminates revealed that internal damage was in the shape of a cone of transverse matrix cracks and delaminations. Scanning electron microscopy revealed that delaminations in most materials showed characteristic hackle marks often associated with Mode II shear delaminations. Resin damage directly in the impacted region was seen to consist of cohesive matrix failures and adhesive failures in the fiber-matrix bond.

Ultrasonic techniques were helpful in analyzing patterns of internal damage. Conventionally used C-Scan techniques, though useful in delineating the relative damage resistances of the different materials studied, fail to provide a complete picture of the internal damage state. The characteristic damage state after impact consisted of wedge shaped delaminations spiralling through the thickness at each ply interface and causing the formation of numerous interconnected sublaminates. The ultrasonic evaluation technique used in this study could also provide a quick and effective alternative to destructive and time consuming deplying techniques.

Examinations of post-impact compressive samples revealed that, depending on the material, damage propagated in two different modes. These were delamination growth and localized shear failure. Though final failure invariably involved buckling of one or more of the impact induced sublaminates, the growth of these sublaminates occurred by either delamination propagation (thermosets) or by localized transverse shear band formation (thermoplastics). Both modes are important as they cause severe degradation of post-impact compressive strength.

ACKNOWLEDGEMENTS

This work was supported in part by NASA Grants NAG - 1 - 569 and NAG - 1 - 1063.

REFERENCES

1. K. Srinivasan, W.C. Jackson, and J.A. Hinkley. NASA TM 102755 (1991).
2. K. Srinivasan, W.C. Jackson, and J.A. Hinkley. Proceedings of the 36th International SAMPE Symposium / Exhibition, pp 850 - 862 (1991).
3. J. G. Williams. NASA TM 85756 (1984).
4. B.T. Smith, J.S. Heyman, A.M. Buoncristiani, E.D. Blodgett, J.G. Miller and S.M. Freeman. Materials Evaluation, vol. 47, no. 12, pp 1408-1416 (1989).
5. E.F. Dost, L.B. Ilcewicz and J.H. Gosse. Proceedings of the American Society for Composites, 3rd Technical Conference, pp 354 - 363 (1988).
6. A.J. Russell and K.N. Street edited by N.J. Johnston. Toughened Composites, ASTM STP 937. Philadelphia, PA: ASTM, pp 275 - 294 (1987).

LIST OF FIGURES

AUTHOR BIOGRAPHIES

Krishna Srinivasan received his B(Tech) degree from UDCT, Bombay, India and his PhD in Materials Engineering from Rensselaer Polytechnic Institute in 1988. He is currently conducting research on advanced composites while working as a Research Associate with Old Dominion University.

Wade Jackson received his BS degree from Purdue University and his MS degree in Mechanical Engineering from Stanford University in 1990. He works in the Mechanics of Materials Branch at NASA-Langley where he conducts research on advanced composite materials.

Barry T. Smith received his Ph.D. in Physics from the College of William and Mary in 1978. From 1980 to 1989 he was a faculty member of the Physics Department of Christopher Newport College. Currently, he is on the research faculty of the Applied Science Program at the College of William and Mary. As an investigator on grants awarded by NASA, he has conducted research in photoelectrochemisty, surface plasmons, amorphous silicon solar cells, thermodynamic limits of energy conversion by quantum and thermal devices, and most recently the QNDE of composites using ultrasonics and digital signal processing techniques.

Jeffrey Hinkley received his BA degree from Northwestern University and his PhD in Physical Chemistry from the University of Wisconsin in 1978. For the last seven years, he has worked in the Polymeric Materials Branch at NASA-Langley, where his responsibilities include mechanical characterization of polymers and composites.

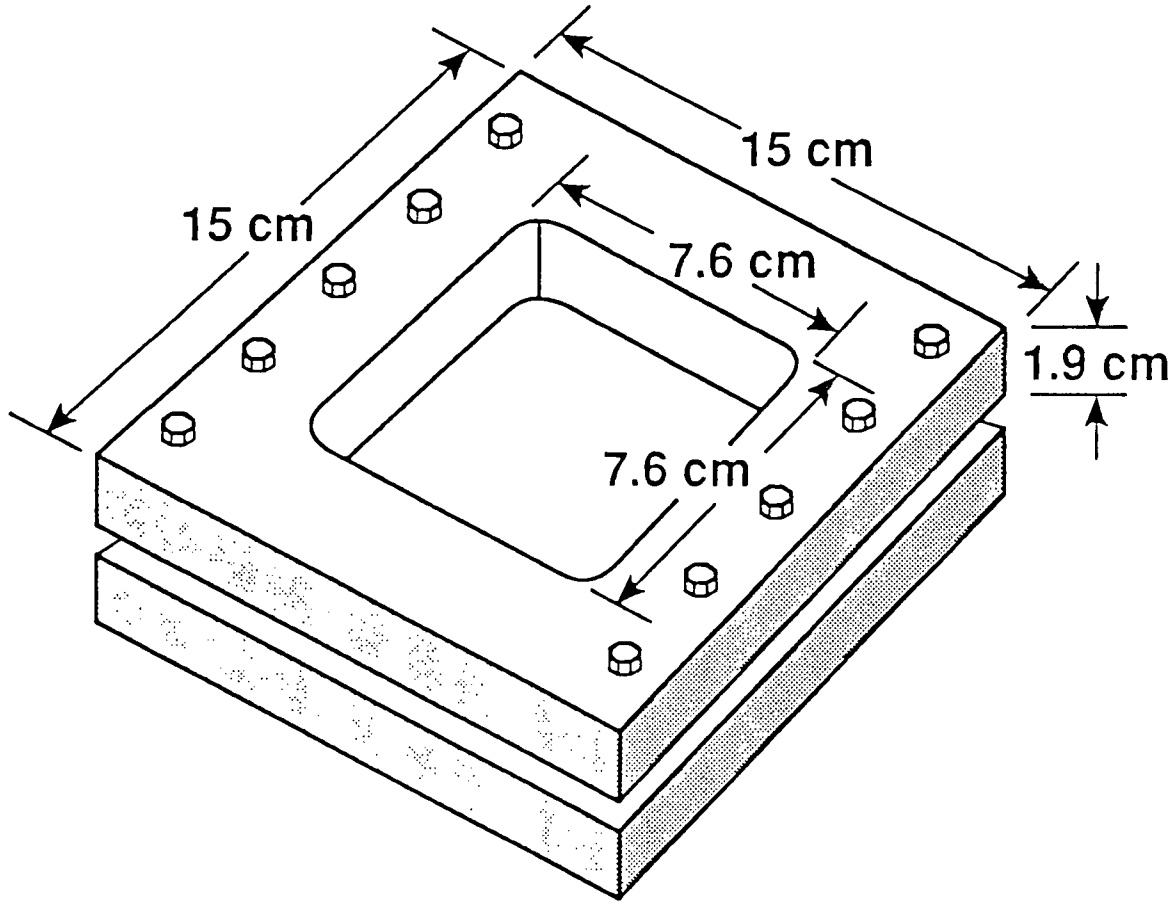
15 cm
15 cm
7.6 cm
7.6 cm
1.9 cm

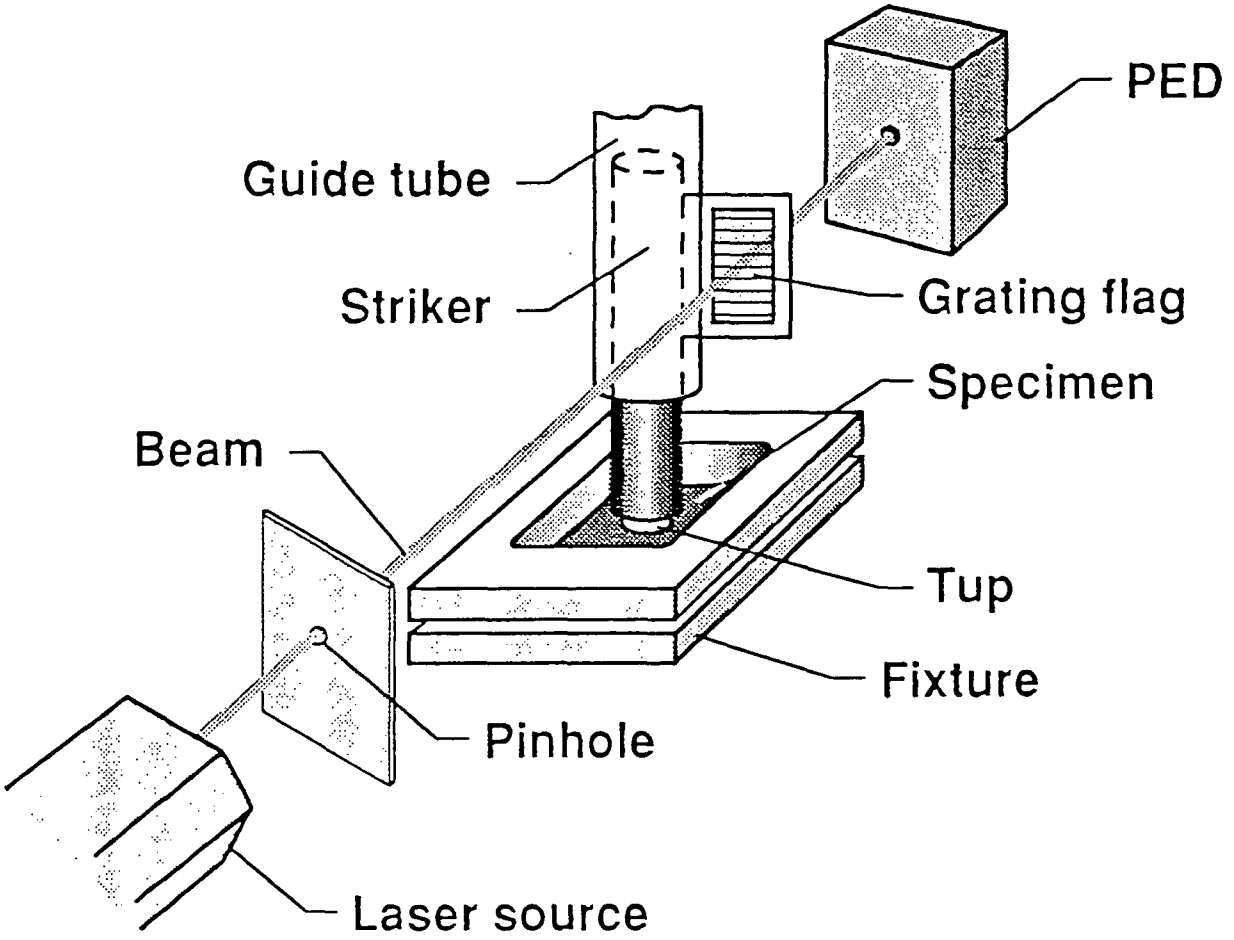
PED
Guide tube
Striker
Grating flag
Specimen
Beam
Tup
Fixture
Pinhole
Laser source

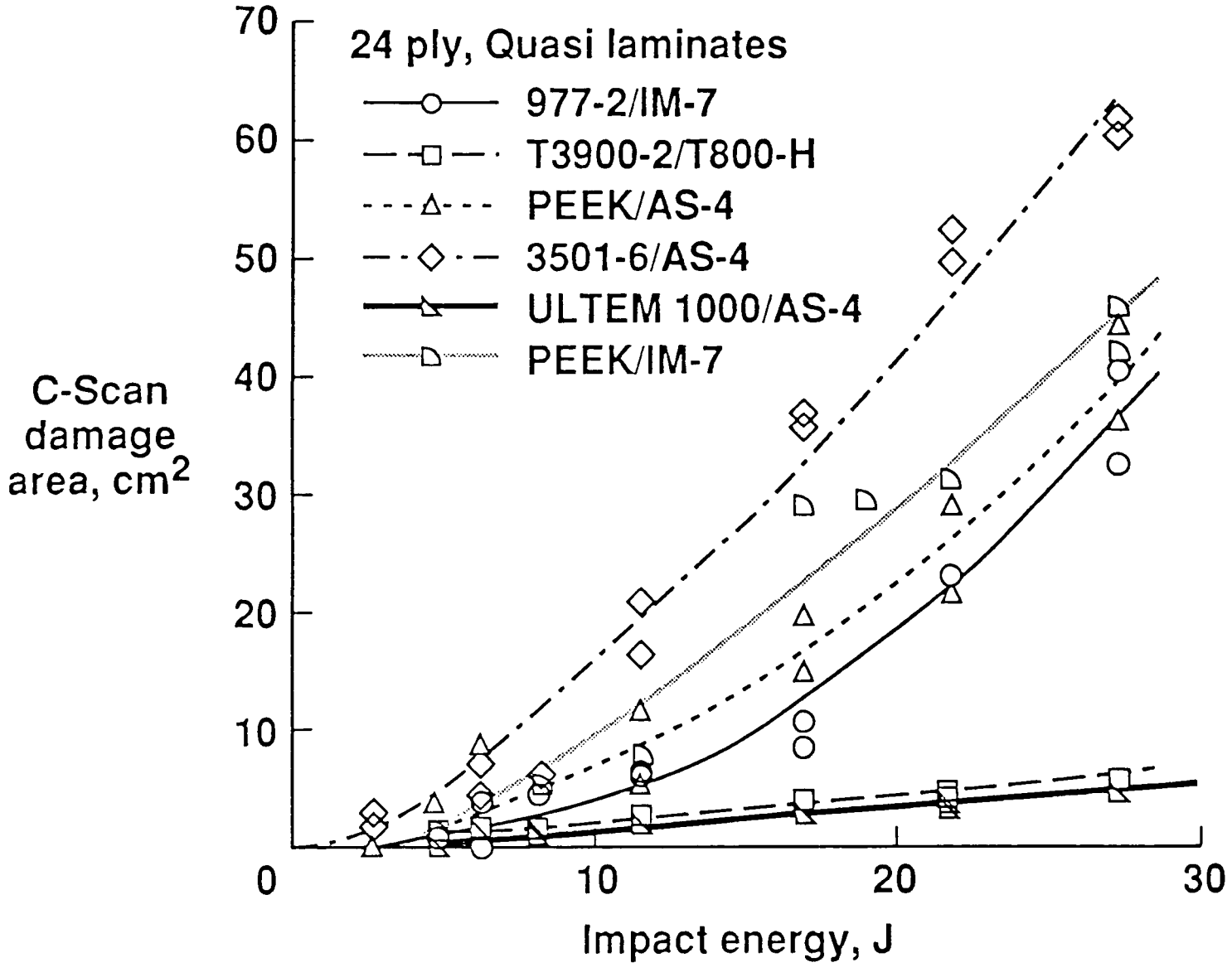
24 ply, Quasi laminates
977-2/IM-7
T3900-2/T800-H
PEEK/AS-4
3501-6/AS-4
ULTEM 1000/AS-4
PEEK/IM-7
C-Scan damage area, cm2
70
60
50
40
30
20
10
0
10
20
30
Impact energy, J

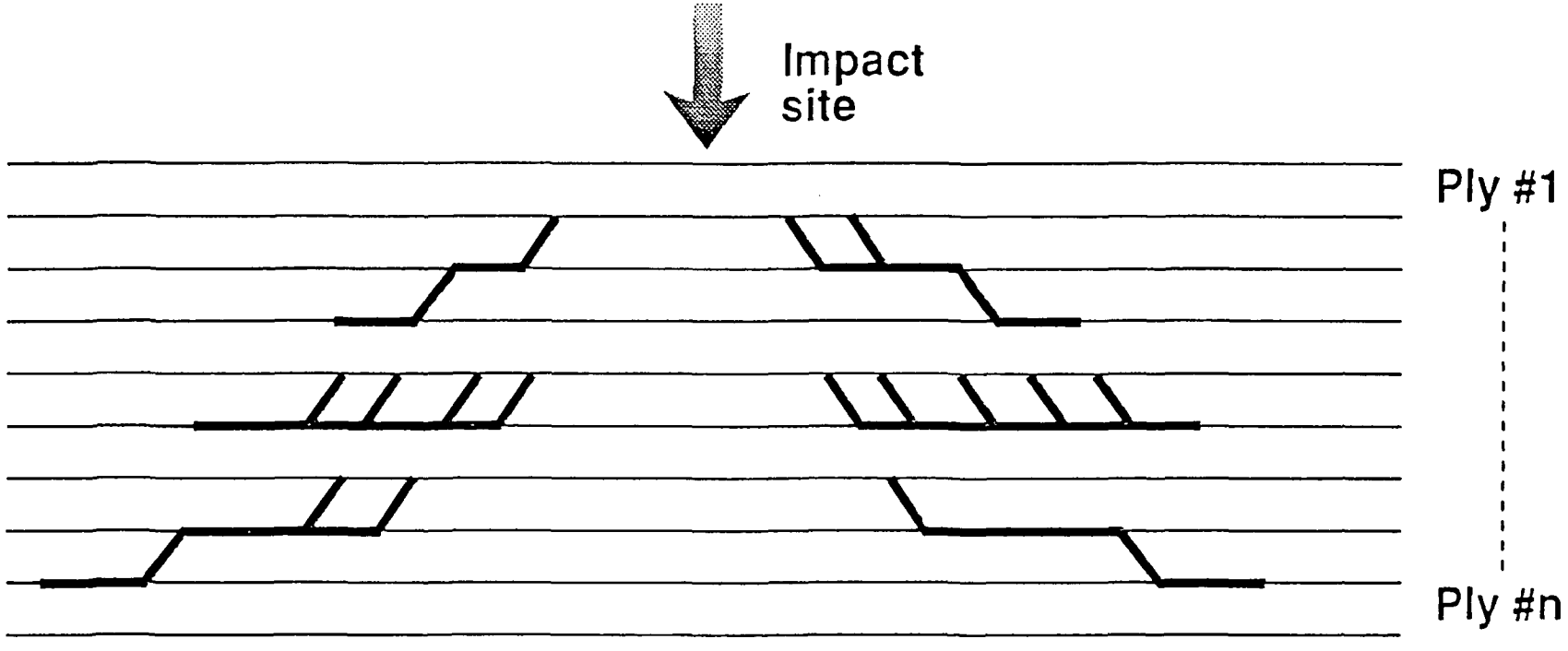
Impact
site
Ply #1
Ply #n

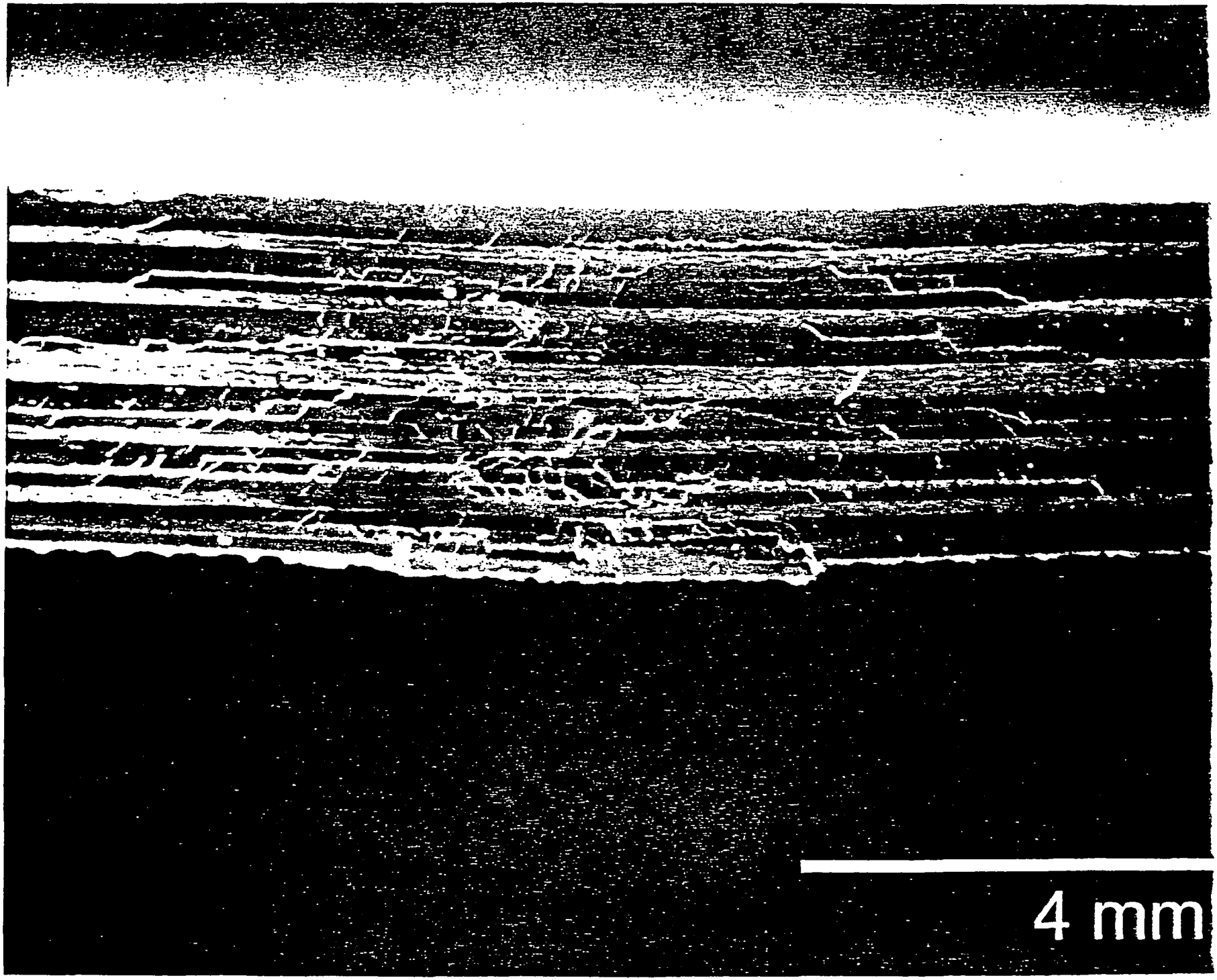
4 mm

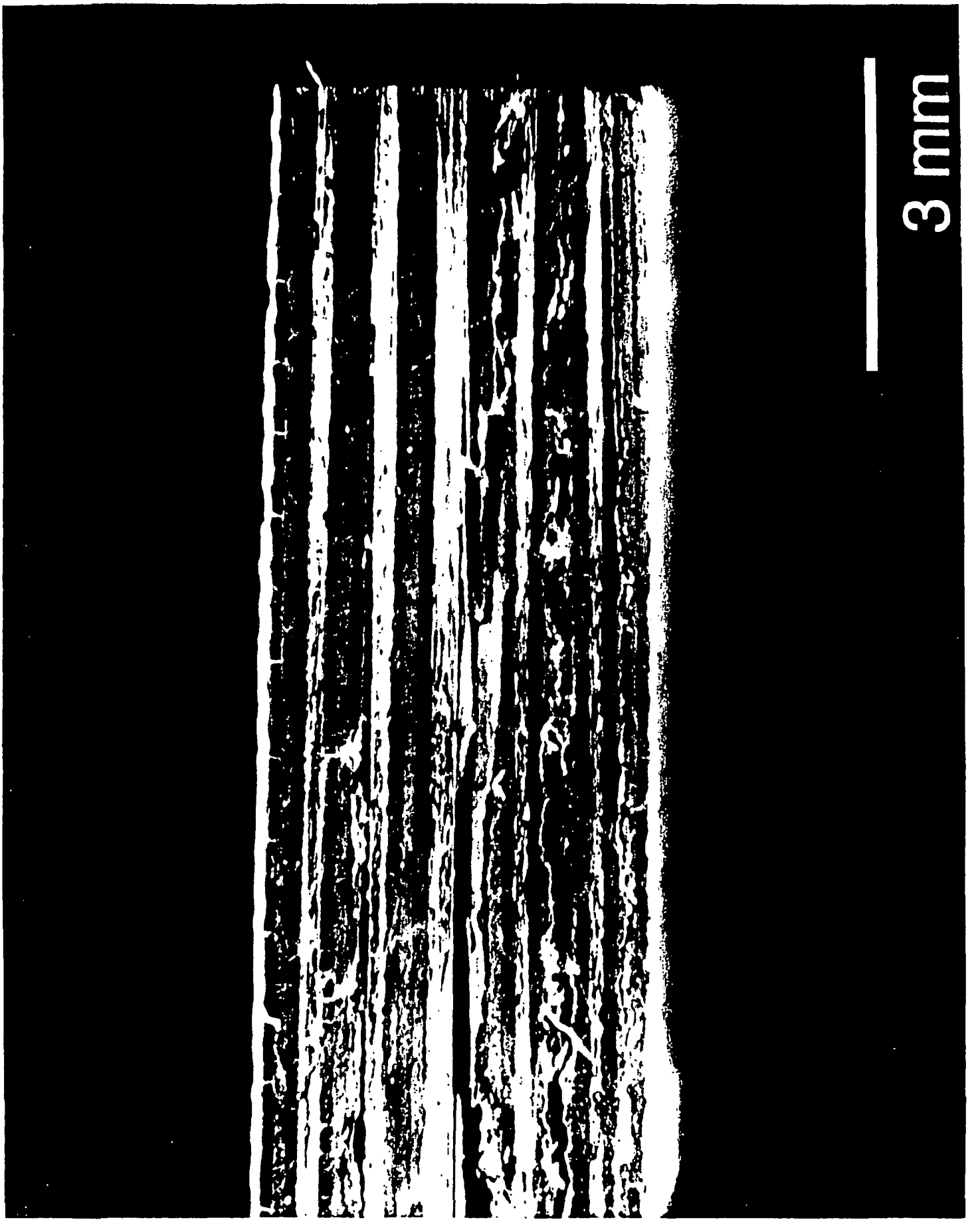

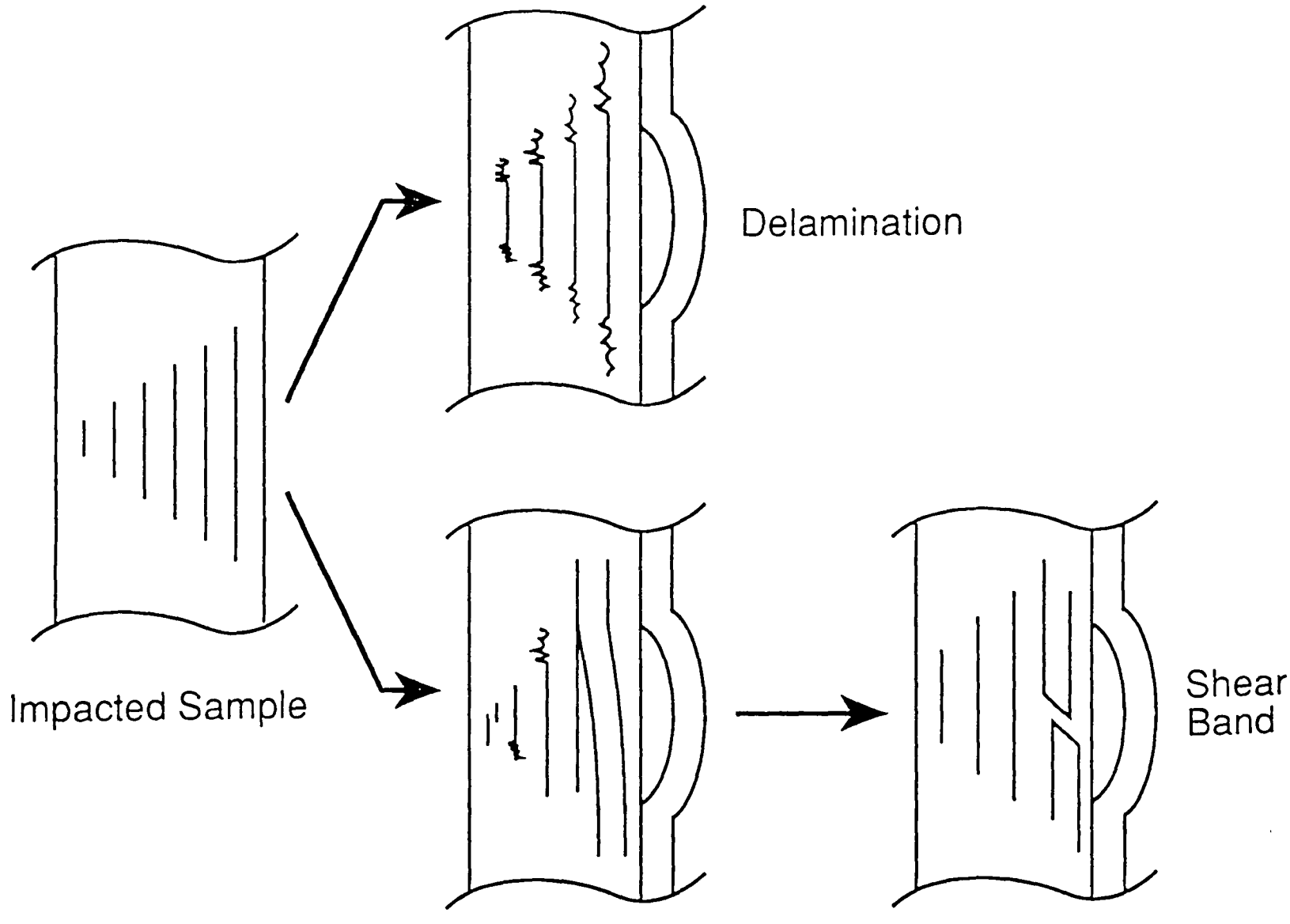
Delamination
Impacted Sample
Shear
Band

(3D_reinf)

COMPRESSION RESPONSE OF THICK LAYER COMPOSITE LAMINATES WITH THROUGH-THE-THICKNESS REINFORCEMENT

Gary L. Farley
U. S. Army Aerostructures Directorate, AVSCOM
NASA Langley Research Center
Hampton, VA 23665-5225

Barry T. Smith *
Applied Science
College of William and Mary
Williamsburg, VA 23185

and

Janice Maiden
Textile Technologies, Inc.
Hatboro, PA 19040

ABSTRACT

Compression and compression-after-impact (CAI) tests were conducted on seven different AS4-3501-6 [0/90] 0.64-cm thick composite laminates. Four of the seven laminates had through-the-thickness (TTT) reinforcement fibers. Two TTT reinforcement methods, stitching and integral weaving, and two reinforcement fibers, Kevlar and carbon, were used. The remaining three laminates were made without TTT reinforcements and were tested to establish a baseline for comparison with the laminates having TTT reinforcement. Six of the seven laminates consisted of nine thick layers whereas the seventh material was composed of 46 thin plies. The use of thick-layer material has the potential for reducing structural part cost because of the reduced part count (layers of material).

The compression strengths of the TTT reinforced laminates were approximately one half those of the materials without TTT reinforcements. However, the CAI strengths of the TTT reinforced

* Work supported in part by NASA grant NAG-1-1063

materials were approximately twice those of materials without TTT reinforcements. The improvement in CAI strength is due to an increase in interlaminar strength produced by the TTT reinforcement. Stitched laminates had slightly higher compression and CAI strengths than the integrally woven laminates.

INTRODUCTION

Cost and damage tolerance are related factors that significantly influence the commercial utilization of composite materials as engineering structures. Using conventional composite fabrication processes, large primary composite structures for commercial aircraft applications are more expensive than comparable metallic structure. Improvement in damage tolerance has been achieved by using "tougher" matrices, however these materials are more expensive than the less damage tolerant, brittle composite materials, [1].

Research is being supported by both government and industry to develop cost effective and damage tolerant composite materials through the exploitation of textile technology. Weaving [2-7], stitching [1, 8-15], braiding [16-24] and knitting [25, 26] are being evaluated as methods to produce dry fiber preforms because of the high degree of automation inherent in the textile process and the potential for improvement in damage tolerance using 3-D fiber architectures. Furthermore, 3-D fiber architectures afford a potential to tailor the level of damage tolerance using inexpensive matrix materials.

Large filament count yarns used as in-plane reinforcements have the potential for reducing fabrication costs. The larger the filament count of the yarn, the fewer machine operations required to produce the same quantity of material; thus a less expensive material. Furthermore, large filament count yarns are less expensive than small filament count yarns for the same quantity of fiber.

The objective of this research is to evaluate the compression and compression-after-impact response of 0.64-cm thick composite [0/90] laminates with stitched and integrally woven through-the-thickness (TTT) fiber architectures fabricated from dry fiber preforms. This investigation will provide trend information about how different TTT reinforcement methods, layer thickness, impact methods and impact energy influences strength, failure modes and failure mechanisms. Although the [0/90] fiber architecture is not normally considered a structural material because of the lack of off-axis plies, it is the only fiber orientation where a direct comparison between stitched and integrally woven materal forms can be made. Specimens without TTT reinforcements were also fabricated and evaluated for comparison with laminates that have TTT reinforcement.

LAMINATES

Seven different laminate configurations were evaluated in this investigation. Two of the laminates consist of nine plies of dry uniweave fabric having a [0/90/0/90/0/90/0/90/0] ply orientation stitched TTT with either T-900-1000A Toray carbon or 1100 denier Kevlar-

49 yarn. The uniweave fabric is a fabric with a large percentage (in this case greater than 99 percent by weight) of warp yarns held together with small denier glass fill yarns. The carbon warp yarns were a 21K filament AS4 yarn and were positioned approximately five yarn bundles (ends) per centimeter. The 21K yarn was used because of the harness capability of the loom and the desired preform geometry and architecture. The 21K yarn was created by combining 3K, 6K and 12K yarns. The stitched TTT reinforced laminates employed a modified lock stitch in orthogonal directions relative to the 0 degree direction of the laminate. Stitch row spacing was 0.64 cm and stitch pitch was 0.32 cm, as illustrated in Fig. 1. The stitched TTT reinforcement penetrates in-plane yarns and some fiber breakage occurs at each stitching needle penetration.

Two nine ply [0/90/0/90/0/90/0/90/0] dry fiber preforms with integrally woven TTT reinforcement yarns were also evaluated in this investigation. The in-plane carbon yarns were the same 21K AS4 yarns used in the stitched preforms. These yarns were spaced approximately five ends per centimeter. In this woven preform there was no interlocking between adjacent layers. Through-the-thickness reinforcement yarns were integrally woven starting at the upper or lower surface and extended into the center of the preform and looped around a catcher yarn, as depicted in Fig. 1. The same carbon and Kevlar TTT reinforcement yarns and orthogonal reinforcement pattern used in the stitched preforms were used in the integrally woven preforms. The integrally woven TTT yarns were positioned between the in-plane yarns.

Three different sets of specimens without TTT reinforcement were tested and used for comparison with the specimens having TTT reinforcement. These sets consisted of a nine layer [0/90] uniweave material and two sets fabricated from tape prepreg. The uniweave material is the material used in the stitched preforms and is similar to the in-plane fiber architecture of the integrally woven material. The ply orientation of all materials without TTT reinforcement was [0/90/0/90/0/90/0/90/0]. All of the dry fiber preforms, with and without TTT reinforcement, were infiltrated with 3501-6 epoxy resin using a vacuum infiltration technique [13] and cured using the same resin-manufacturer-recommended time-temperature-pressure profile as used for the prepreg materials.

The two other laminates without TTT reinforcement were fabricated from AS4/3501-6 tape prepreg and had ply orientations of $[(0_5/90_5)_2/0_3]_S$ and $[(0/90)_2/0/(0/90)_5/0/(0/90)_3/0]_S$ which are denoted as the "thick-layer" and "thin-layer" materials, respectively. The cured laminate thickness were similar to the thickness of laminates fabricated from the dry fiber preforms. Multiple prepreg plies having the same orientation were positioned together in the "thick-layer" material to simulate the thick-layers in the stitched and integrally woven laminates. The "thick-layer" material did not have the TTT reinforcement and fiber crimp/waviness produced by the textile process. The "thin-layer" laminate has an alternating stacking arrangement of plies. Alternating the ply orientation of adjacent layers reduces interlaminar stresses. Reducing interlaminar stresses can produce higher laminate strength than

when multiple layers of the same ply orientation are positioned together.

The [0/90] fiber architecture used in this investigation is not generally used in practical engineering structures because of its low in-plane shear stiffness and strength, but it is useful for investigating failure mechanisms and the mechanics of TTT reinforcement because of the reduced complexity of the stress state in the material. A secondary reason for using the [0/90] architecture is that current loom capabilities are limited to the [0/90] fiber orientation, however it is expected that future textile machines, such as looms, will be able to integrally incorporate off-axis fibers to provide the necessary shear properties. Therefore, the [0/90] materials evaluated in this study facilitates investigating some of the merits and deficiencies of integrally weaving TTT reinforcement into preforms prior to the development of new textile machines.

Fiber volume fractions were measured on samples of all seven materials using ASTM D-3171 acid digestion method, [27]. Nominal fiber volume fractions for all specimens are tabulated in Table 1. The reported fiber volume fraction is the total fiber volume fraction including any TTT reinforcement. Fiber volume fractions ranged from 55.2 to 63.5 percent. Since there was a considerable range in values, all failure load and strength values are reported as normalized to a 60 percent fiber-volume fraction.

TEST SPECIMENS

Short-block-compression (SBC) specimens were used in this investigation to measure the undamaged compression strength of the materials. Short-block-compression specimens, depicted in Fig. 2, are 4.45 cm high by 3.81 cm wide by 0.64 cm thick with the 3.81-cm sides ground flat and parallel, specimen geometry and strength data are presented in Table 1. Test specimens were mounted in a test fixture and the specimen-fixture assembly placed in a conventional hydraulic test machine. All specimens were tested in the 0 degree direction. Prior to each test the load plattens of the test machine were positioned such that any initial bending induced in the specimen was minimized.

Residual compression strength after damaged was evaluated using compression-after-impact specimens that were 12.7 cm wide by 25.4 cm in length by approximately 0.64 cm thick, as depicted in Fig. 2. The 12.7-cm wide sides were grounded flat and parallel. Each specimen was impacted in the center on one side with either a 1.27-cm diameter aluminum ball propelled by an air gun [7] or impacted by a weighted 1.27-cm diameter tup in a drop weight impactor [28]. Impact energy levels ranged between 13 J and 68 J. After impact, each CAI specimen was ultrasonically scanned to determine the surface and internal damage. Specimen geometry, damage area, damage width, damage length, impact energy and compression strength data are listed in Table 2. The CAI specimens were mounted in a side-supported-compression fixture and the specimen-fixture assembly placed into a conventional hydraulic test machine. The plattens of the test machine were set to minimize any

initial bending strains in the CAI specimen. Each specimen was statically loaded in the 0 degree direction until failure.

DAMAGE ASSESSMENT

The damaged area and the width and length of the damaged region of each CAI specimen were measured using ultrasonic imaging techniques. Damage width and length refer to length of damage relative to the 12.7 cm and 25.4 cm dimensions of the specimen, respectively. The damaged area, width and length were measured from a conventional C-scan image. However, impact-induced damage varies with depth into the specimen and conventional C-scans do not distinguish the damage as a function of depth. Typical damage at an interface (illustrated in Fig. 3) consists of delamination between adjacent plies and crushed material beneath the point of impact. This damage region resembles a dumbbell at an interface and the size of the damaged region can increase from the impacted (front) surface to the back surface. Also, the dumbbell shaped damage region changes orientation depending upon the fiber orientation of the adjacent layers [29].

The ultrasonic evaluation was performed in a water bath using a 5 MHz transducer with a 1.27-cm aperture and a 5.08-cm focal point. The transducer was operated in a pulse-echo mode and was excited with a square wave pulser. The return signal was amplified and fed into a time-gain-compensated amplifier. A digitizer with sampling rate of 50 MHz and 8 bit dynamic range acquired the signal and passed it to a computer for later analysis. The entire ultrasonic wave was digitized

to include the front, interior, and back surface reflections. A spatial sampling step of 2 mm was on the order of the 6 dB point spread for the transducer as determined experimentally.

RESULTS AND DISCUSSION

Short-block-compression strength

Short-block-compression specimens were fabricated from all seven different materials. Their strengths are presented in Fig. 4. The "thin-layer" tape prepreg specimens had the highest compressive strength of 885 MPa followed by the uniweave and "thick-layer" tape prepreg at 654 MPa and 592 MPa, respectively. A 33 percent strength reduction, as seen in Fig. 4, was obtained for the "thick-layer" laminates as compared to the "thin-layer" laminates. The strength reduction is attributed to increased layer thickness because the difference between the "thin-layer" and "thick-layer" laminates is the stacking sequence. Even though the uniweave material had comparable ply thickness as the "thick-layer" material, the uniweave material experienced a somewhat smaller (26 percent) reduction in compressive strength compared to the "thin-layer" material. Both the "thick-layer" and uniweave materials exhibited a combination of interlaminar cracks and transverse shear failure, as seen in Fig. 5.

The differences in compressive strength between the "thick-layer" and uniweave materials can be partially attributed to the difference in fiber architecture. That is, the fiber architecture in each layer of

the uniweave fabric has fine denier glass fill yarns used for handleability of the dry uniweave fabric. As a part of the composite laminate, the glass fill yarn provides lateral support to the warp yarns in an analogous manner as the matrix. As lateral support to the warp yarns increase the adverse influence of fiber waviness decrease, hence an increase in compression strength for the uniweave laminates.

Waas [30] has shown that the thicker a ply the shorter the fiber microbuckle wave length. The shorter the wave length the greater the ratio of the wave applitude to wave length and hence, the lower the compressive strength [31]. Based upon analysis, a strength reduction of up to 50 percent is possible due to fiber waviness, [31]. Fiber waviness adversely influence the interlaminar stresses that are created in a laminate at free edges, around local imperfections and at discontinuities. Therefore, it is believed the reduced compressive strength of both the "thick-layer" and uniweave laminates, as compared to the "thin-layer" laminate, is related to fiber waviness.

The thick-layer laminates with TTT reinforcement exhibited significant reductions in compressive strength as compared to the laminates without TTT reinforcement. These strength reductions were on the order of 45 to 55 percent compared to the "thin-layer" material (see Fig. 4), and 30 to 45 percent compared to the uniweave material. Thin-layer quasi-isotropic laminates with TTT reinforcements were evaluated, [1], and the compression strength reduction as a percent of the compression strength of laminates without TTT reinforcements was approximately one half of the reduction measured for the specimens tested in this investigation.

These strength reductions, relative to the "thin-layer" and uniweave materials, can be attributed to: 1) the surface loop yarn of the TTT reinforcement kinking the in-plane fibers near the surface [32], 2) a decrease in the distance between filaments within a yarn bundle, 3) in-plane fiber waviness created by the inclusion of TTT (see Fig. 6), and 4) fiber breakage as a result of stitched TTT yarn insertion [33].

Based upon costs of yarns having filament counts of between 1K and 12K, the fiber costs of a comparably produced 21K yarn would be approximately 20 percent of the cost of 3K yarns. Loom setup and operation time would decrease by a factor of 7 when the 21K yarn is used instead of the 3K yarn. Therefore, significant costs savings for structures utilizing both thick-layer material and TTT reinforcement are potentially achievable even though the undamaged compression strength is less. If the design of a structure was driven more by cost than by undamaged compression strength, then significant benefit could be achieved by using thick-layer laminates with TTT reinforcements. A comprehensive study focusing on structural performance and cost of these types of materials is warranted to understand the relationship between structural performance and cost.

The laminate with integrally woven TTT reinforcement exhibited a slightly lower compression strength than the stitched laminates for both Kevlar and carbon TTT reinforcements, as depicted in Fig. 4. Strength differences are attributed to differences in the TTT fiber architecture of these materials. In the stitched laminate the TTT reinforcement penetrated yarn bundles which formed an elliptically shaped matrix-rich

region around the TTT reinforcement, as seen in Fig. 6. The integrally woven TTT reinforcement is positioned between the in-plane yarns which separates the in-plane yarns forming matrix-rich channels, see Fig. 6. Formation of these matrix-rich channels reduce the matrix in the yarn bundles as compared to a stitched material with the same total fiber volume fraction, as observed in Fig. 7. Reducing the matrix in the in-plane yarn bundles lessens the distance between filaments which increases the stress in the matrix around the filaments, [34 and 35], for the same applied load to the laminate. The increase in stresses around the filaments reduces the stiffness of the matrix through plastic deformation which reduces the lateral support provided by the matrix to the in-plane fibers. Reducing lateral support to the axial fibers promotes lateral movement of the axial fibers which can decrease compression strength of the laminate.

A measure of damage severity

Compression-after-impact strength is frequently reported as a function of either impact energy or damage area. When CAI strength is plotted as a function of impact energy or damage area, such as the test data from this investigation depicted in Figs. 8 and 9, a significant data scatter is observed because impact energy or damage area is not related to the mechanism that controls failure of the specimen. Hence, it is more appropriate to correlate, if possible, strength as a function of parameters that are related to the mechanisms that control the failure process.

The macroscopic failure modes of CAI specimens are typically either an interlaminar crack growth, see Fig. 10, or a transverse shear failure, see Fig. 10. Interlaminar crack growth is caused by the buckling/bending of delaminated layers in the damaged region and is a function of the current delamination length. The longer the delamination, the lower the load required to buckle/bend the delaminated layer(s) and, hence, promote crack growth. Therefore, the failure load of CAI specimens that exhibit extensive interlaminar crack growth is a function of damage length.

Little interlaminar crack growth occurs in specimens that exhibit exclusively a transverse shear failure. Load is principally carried around the damaged region through the undamage portion of the specimen. This failure mode is caused by the eccentric load path developed due to the conical shaped (through the thickness) impact damage. The eccentric load produces a local bending moment which causes the transverse shear failure mode. Therefore, the failure of specimens that exhibit transverse shear failure is proportional to the undamaged width of the specimen.

The CAI strength of specimens tested in this investigation were plotted as a function of damage width and damage length (see Figs. 8 and 9), giving a reduced data scatter. Damage length as the independent variable most noticably reduced the scatter for those specimens without TTT reinforcement. These specimens exhibited mostly delamination induced failures for which, as previously described, the failure load is a function of damage length. There was little visual difference between

representing the data with TTT reinforcement as a function of damage width or length because damage width and length were similar, see Table 2. Specimens with TTT reinforcements failed in a transverse shearing mode.

To quantify which parameter, damage length or width, correlates better with CAI strength a linear regression analysis was performed and the corresponding square root of the coefficients of determination of the data presented in Figs. 8 and 9 was evaluated, see table 3. Coefficient of determination can be used as a measure of data scatter, that is, the closer the coefficient of determination is to 1.0 the less data scatter. Based upon the coefficient of determination, damage length seems to be the better correlating parameter of the four considered (impact energy, damage area, damage width, and damage length) because the data scatter was clearly reduced. It is conceivable that damage width could be the better correlating parameter for other materials. All further reference in this paper to damage refers to damage length unless otherwise stated.

Influence of impact method

There are two commonly used methods of producing impact damage in composite specimens, the air gun and the drop weight. A bar graph showing damage lengths for different laminates and impact energy levels is presented in Fig. 11. Materials without TTT reinforcement were impacted with approximately 14 J and 40 J of energy using air gun and drop weight methods. The air gun generally produced a greater damage for approximately the same impact energy than did the drop weight.

Similar damage trends for air gun and drop weight impacts were obtained for specimens with TTT reinforcement, as depicted in Fig. 12. In all cases the air gun produced slightly more damage than the drop weight for all laminates investigated.

The measured CAI strengths of these materials is consistent with damage produced by the impact, as depicted in Fig. 13. That is, as the impact damage increased the CAI strength decreased. Also, in general, the CAI strengths of specimens impacted with the air gun are slightly lower for approximately the same energy level impact than the specimens impacted with the drop weight (Figs. 13 and 14), a finding consistent with the air gun producing slightly greater damage.

Influence of TTT reinforcement

As shown in Fig. 4, the compression strength of the laminates with TTT reinforcement was approximately one half that of those materials without TTT reinforcement. However, when impacted at approximately 40 J with either an air gun or drop weight, the CAI strength of the TTT reinforced materials was approximately 25 to 50 percent higher than materials without TTT reinforcement, see Figs. 15 and 16. This dramatic reversal in the structural performance of these materials is consistent with published results for other materials and ply orientations [8, 11 and 12]. Therefore, a structure principally designed by laminate CAI strength utilizing thick-layer material with TTT reinforcement realizes no significant penalty in structural performance. Furthermore,

combining thick-layer material with TTT reinforcement, has the potential for significantly reducing fabrication costs as previously discussed. Further study of the performance and cost of these material forms is warranted.

The specimens with stitched TTT reinforcements exhibited slightly higher CAI strengths than the same materials with integrally woven TTT reinforcements. Small differences in strengths were obtained for the Kevlar or carbon TTT reinforcement. Hence, it apprears that both the Kevlar and carbon fibers provided similar interlaminar strength to limit the impact induced damage.

At the impact energy levels used in this investigation, impact-induced damage was comprised of crushed material and inter/intralaminar delaminations. At the impact point on the surface of the specimen the damage consisted primarily of crushed material with some delamination between plies at the first interface. As shown in the B-scan images in Fig. 17, a cone of damage formed beneath the point of impact. The amount of crushed material decreased with increasing depth into the specimen whereas the interlaminar delaminations increased with depth. In specimens without TTT reinforcement the damage cone angle increased with ply thickness and the greatest damage occurred at the back surface of the specimen. Through-the-thickness reinforcement decreased the cone angle and reduced the damage. The damage area of materials with TTT reinforcements remaind nearly constant through the thickness over 75 percent of the laminate depth.

SUMMARY REMARKS

The compression strengths and compression-after-impact (CAI) strengths of seven different AS4/3501-6 [0/90] composite laminates were measured in this investigation. Four of these laminates were fabricated with through-the-thickness (TTT) reinforcements while the remaining three laminates had no TTT reinforcements. Two TTT reinforcing methods, stitching and integral weaving were employed and two reinforcement yarns, Kevlar and carbon, were used. The compression and CAI strength trends of the laminates with TTT reinforcements were consistent with prior research. That is, thick-layer laminates with TTT reinforcements exhibited twice the reduction in undamaged compression strength as previously reported thin-layer laminates with TTT reinforcements. However, the improvement in CAI strength of thick-layer laminates with TTT reinforcements as a percent of the CAI strength of thin-layer laminates without TTT reinforcement was comparable to previously reported CAI strength improvements obtained for thin-layer laminates with TTT reinforcements. Therefore, no significant penalty in CAI strength occurs for thick-layer materials with TTT reinforcements.

There is a potential significant reduction in cost of composite structures with no significant loss in CAI strength that is achieveable by utilizing thick-layer materials with TTT reinforcements. However, the lower costs must be balanced against lower undamaged compression strength. If in the structural design of a part the design requirements are closely related to the CAI strength of the laminate then a lower cost structure can be realized utilizing thick-layer materials with TTT

reinforcements. A comprehensive study is warranted to investigate the structural performance and cost of thick-layer materials with TTT reinforcements.

The stitched materials produced slightly higher compression and CAI strength than the integrally woven TTT reinforced materials even though the TTT architectures were similar. This difference in strength is attributed to the formation of matrix-rich channels in the integrally woven TTT reinforced materials which reduced the matrix volume fraction in each in-plane yarn. Reducing matrix volume fraction increased the stresses in the matrix around the fibers reducing the lateral support to the axial fibers which reduces the compression strength of the laminate. Therefore, the integrally woven laminates fail at a lower strength than stitched laminates.

As per ply thickness increases, compression and CAI strengths of materials without TTT reinforcements decrease. The decrease in strength is believed to be due to higher interlaminar stresses. The inclusion of TTT reinforcements provides sufficient interlaminar strength that the interlaminar effects were negated for the CAI specimens.

Compression-after-impact strength was found to correlate better with damage length than with impact energy, damage area or damage width in that the data scatter was significantly reduced when CAI strength was plotted as a function of damage length. It is proposed that the reason for this improved correlation is because damage length is related to the failure mechanisms exhibited by these materials.

REFERENCES

1. Dow, M.B., Smith, D. L. and Lubowinski, S. J., "An Evaluation of Stitching Concepts for Damage-Tolerant Composites", NASA CP 3038, 1989.

2. Dow, N. F. and Ramnath, V., "Analysis of woven fabrics for reinforced composite materials", NASA CR 178275, April, 1987.

3. Dexter, H. B. and Maiden, J., "Application of Textile Material Forms To Composite Aircraft Structures", NASA CP 3001, 1988.

4. Zawislak, S. P. and Maiden, J. R., "Advanced Weaving Concepts for Complex Structural Preforms", NASA CP 3038, 1989.

5. Lynch, T., "The Fabrication of Low-Cost Structural Shapes For Composite Reinforcement", NASA CP 2420, 1986.

6. Craford, J. A., "Recent Developments in Multidirectional Weaving", NASA CP 2420, 1986.

7. Smith, D. L. and Dexter, H. B., "Woven Fabric Composites With Improved Fracture Toughness and Damage Tolerance", NASA CP 3038, 1989.

8. Dexter, H. B. and Funk, J. G., "Impact Resistance and Interlaminar Fracture Toughness of Through-the-Thickness Reinforced Graphite/Epoxy", AIAA paper 86-1020-LP, May 1986.

9. Sun, C.T. and Miller, L., "The use of Stitching to Suppress Delamination in Laminated Composite,", ASTM STP-876.

10. Sawyer, J. W., "Effect of Stitching on the Strength of Bonded Composite Single Lap Joints", AIAA Journal 23,11, Dec. 1985.

11. Pelstring, R. M. and Madan, R. C., "Stitching to Improve Damage Tolerance of Composites", presented at the 34th International SAMPE Symposium May 8-11, 1989, Book 2 of 2.

12. Dow, M. B. and Smith, D. L., "Damage-Tolerant Composite Materials Produced by Stitching Carbon Fabrics", Proceedings of 21st International SAMPE Technical Conference, Atlantic City, NJ, Sept. 1989.

13. Palmer, R. and Curzio F., "Cost-Efective Damage-Tolerant Composites Using Multi-Needle Stitching and RTM/VIM Processing", NASA CP 3038, 1989.

14. Drummond, T. and Krasnitz, R., "Advanced Stitching Technology for the Composite Industry", NASA CP 3082, 1990.

15. Hotz, L. E., "Application of Quilting and Stitching Technology", NASA CP 3082, 1990.

16. Stinchcomb, W., Simonds, R. A. and Jones, R. M., "Mechanical Behavior of Braided Composites", NASA Conference Publication 2420, November 1985.

17. Gause, L. W. and Alper, J. M., "Structural Properties of Braided Graphite/Epoxy Composites", Journal of Composites Technology and Research, V9, n4, Winter 1987.

18. Li. W., Hammad, M. and El-Shiekh, A., "Effect of Braiding Process on the Damage Tolerance of 3-D Braided Graphite/Epoxy Composites", presented at the 34th SAMPE Symposium and Exhibition, May 8-11, 1989, Book 2 of 2.

19. Li, W., Kang, T. J. and El Shiekh, A., "Structural Mechanics of 3-D Braided Preforms For Composites Part I: Geometry of Fabric Produced by 4-Step Process", NASA CP 3001, 1988.

20. Li, W., Hammad, M. and El-Shiekh, A., "Automation and Design Limitations of 3-D Braiding Processes", NASA CP 3082, 1990.

21. Hess, J. P., "Two-Dimensional Braided composite Materials and Structures", NASA CP 3082, 1990.

22. Macander, A., "Multidimensionally Braided Composite Marine Propeller", NASA CP 2420, 1986.

23. Weller, R. D., "AYPEX: A New Method of Composite Reinforcement Braiding", NASA CP 2420, 1986.

24. Brown, R. T., "3-D Braiding: From the Laboratory To The Factory", NASA CP 2420, 1986.

25. Schooneveld, G. V., "Potential of Knitting/Stitching and Resin Infusion For Cost-Effective Composites", NASA CP 3038, 1989.

26. Ko, F. K., "Manufacturing, Structure and Properties of Multiaxial Warp Knit Composites", NASA CP 3082, 1990.

27. "Test of Fiber Content of Resin-Matrix Composites by Matrix Digestion", Annual Book of ASTM Standards," Part 36, D 3171-76, 1982.

28. Standard Tests for Toughened Resin Composites - Revised Edition. NASA RP-1092, July 1983.

29. Smith, B. T., Heyman, J. S., Buoncristiani, A. M., Blodget, E. D., Miller, J. G. and Freeman, S. M., "Correlation of the Deply Technique with Ultrasonic Imagining of Impact Damage in Graphite-Epoxy Composites", Materials Evaluation, Vol. 47, Dec. 1989, pg 1408-1416.

30. Waas, A. M., "Fiber Buckling in Laminated Plates", NASA NAG-1-1040 grant report, June 1990.

31. Shuart, M. J., "An Analysis of Shear Failure Mechanisms for Compression-Loaded $[\pm\Theta]_s$ Laminates", Journal of Composite Materials, vol. 23, March 1989.

32. Farley, G. L., "A Mechanism Responsible For Reducing Compression Strength of Through-The-Thickness Reinforced Composite Materials", Submitted to the Journal of Composite Materials, winter 1991.

33. Portanova, M. A., Poe, C. C. and Whitcomb, J. D., "Open Hole and Post-Impact Compression Fatigue of Stitched and Unstitched Carbon/Epoxy Composites", NASA TM 102676, June 1990.

34. Foye, R. L., "Advanced Design Concepts For Advanced Composite Airframes", AFML-TR-68-91, Volume 1, July, 1968.

35. Foye, R. L. and Baker, D. J., "Design/Analysis Methods For Advanced Composite Structures", AFML-TR-70-199. Feb., 1971.

Table 1. Short-block-compression specimens.

Specimen description	Cross-sectional area, cm^2	Fiber volume fraction, percent		Normalized* strength, MPa	Average strength, MPa
		Total	TTT		
Uniweave					
1	2.33			648.11	
2	2.39	63.5	0	698.46	654.97
3	2.42			618.34	
K stitched					
1	2.42			477.93	
2	2.51	56.5	2.2	421.43	452.03
3	2.48			456.73	
Gr stitched					
1	2.47			398.18	
2	2.47	61.6	2.8	439.38	421.25
3	2.45			426.17	
K woven					
1	2.78			364.36	
2	2.79	59.0	2.6	374.06	363.98
3	2.80			353.54	
Gr woven					
1	2.81			425.77	
2	2.83	56.6	3.3	396.07	400.79
3	2.82			380.54	
Thick layer					
1	2.55			587.03	
2	2.70	57.5	0	580.62	592.79
3	2.71			610.72	
Thin layer					
1	2.54			883.37	
2	2.61	55.2	0	895.29	885.31
3	2.62			877.29	

Thin layer - $[(0/90)_2/0/(0/90)_5/0/(0/90)_3/0]_s$
Thick layer - $[(0_5/90_5)_2/0_3]_s$
Uniweave, stitched and woven - [0/90/0/90/0/90/0/90/0]

* Normalized to 60 percent fiber volume fraction.
TTT - Through-the-thickness fibers

Table 2. Compression-after-impact specimens.

Specimen description	Cross-sectional area, cm^2	Impact method	Impact energy, J	Damage area, cm^2/ width, cm / length, cm	Normalized* strength, MPa
Uniweave 1	7.87	AG	42.34	75.06 / 9.27 / 13.48	134.0
2	7.85	DW	40.67	74.50 / 10.65 / 12.02	168.0
K stitched 1	8.26	AG	42.19	29.01 / 6.08 / 6.20	274.3
2	8.43	DW	40.67	19.05 / 4.52 / 4.74	305.8
Gr stitched 1	8.32	AG	41.73	23.74 / 5.58 / 5.34	267.4
2	8.21	DW	40.67	16.26 / 4.57 / 4.90	251.8
K woven 1	8.90	AG	42.34	26.65 / 6.35 / 5.95	244.2
2	9.02	DW	40.67	22.77 / 5.62 / 5.62	243.0
3	8.96	DW	13.56	8.29 / 3.36 / 3.24	365.7
4	8.65	DW	67.79	30.41 / 5.35 / 6.24	270.7
Gr woven 1	8.56	AG	42.34	32.83 / 6.11 / 6.35	255.4
2	8.79	DW	40.67	20.83 / 4.70 / 5.82	272.6
3	8.33	DW	13.56	9.32 / 3.48 / 3.37	380.8
4	9.12	DW	67.79	30.96 / 5.73 / 7.08	237.2
Thin layer 1	8.88	AG	42.96	25.21 / 4.92 / 8.94	175.6
2	8.85	AG	13.93	11.84 / 3.82 / 4.82	262.8
3	8.88	DW	13.56	20.18 / 5.32 / 5.52	272.3
4	8.91	DW	40.67	24.56 / 5.42 / 8.03	174.9
Thick layer 1	9.04	AG	42.65	71.32 / 8.20 / 15.70	130.2
2	8.96	AG	13.05	30.04 / 5.22 / 9.64	257.4
3	8.91	DW	13.56	29.34 / 6.05 / 8.06	211.7
4	9.01	DW	40.67	45.56 / 7.43 / 8.94	142.5

Thin layer - $[(0/90)_2/0/(0/90)_5/0/(0/90)_3/0]_s$ Thick layer - $[(0_5/90_5)_2/0_3]_s$ AG - Air gun DW - Drop weight

Uniweave, stitched and woven - [0/90/0/90/0/90/0/90/0] * Normalized to 60 percent fiber volume fraction.

Table 3. Square root of coefficient of determination

Impact Method	Impact Energy	Impact Area	Damage width	Damage Length
Air gun	0.38	0.84	0.72	0.90
Drop weight	0.37	0.75	0.79	0.88

Coefficient of determination is based upon a linear regression analysis

Figure 1. Sketches of stitched and integrally woven architectures.

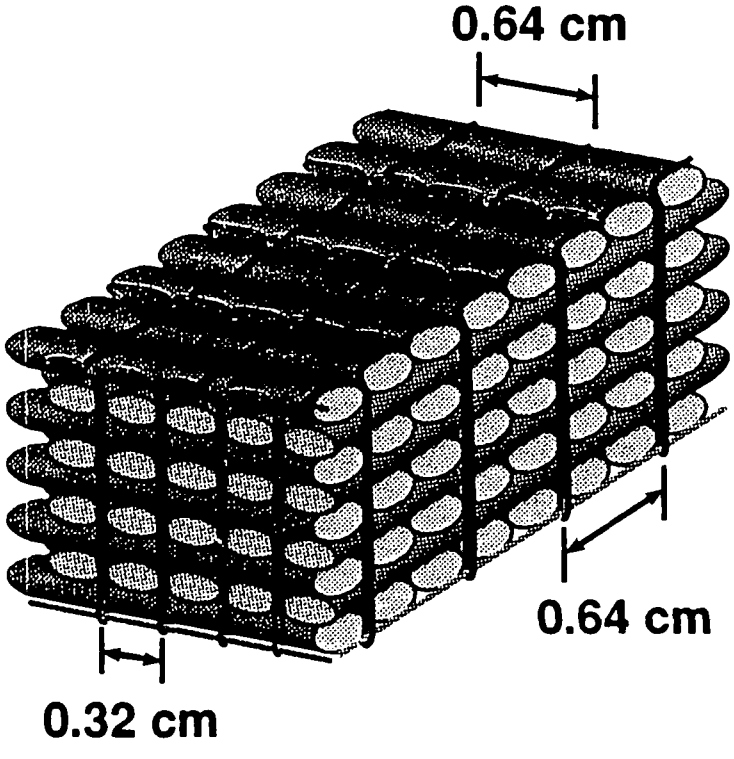

No-crimp stitched

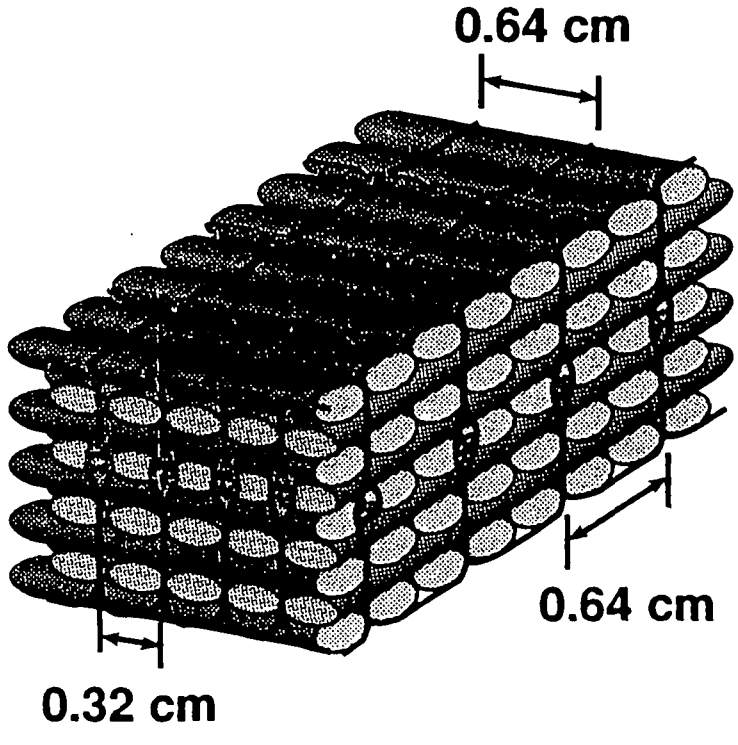

Integrally woven 3-D weave

SHORT-BLOCK-COMPRESSION AND COMPRESSION-AFTER-IMPACT SPECIMENS

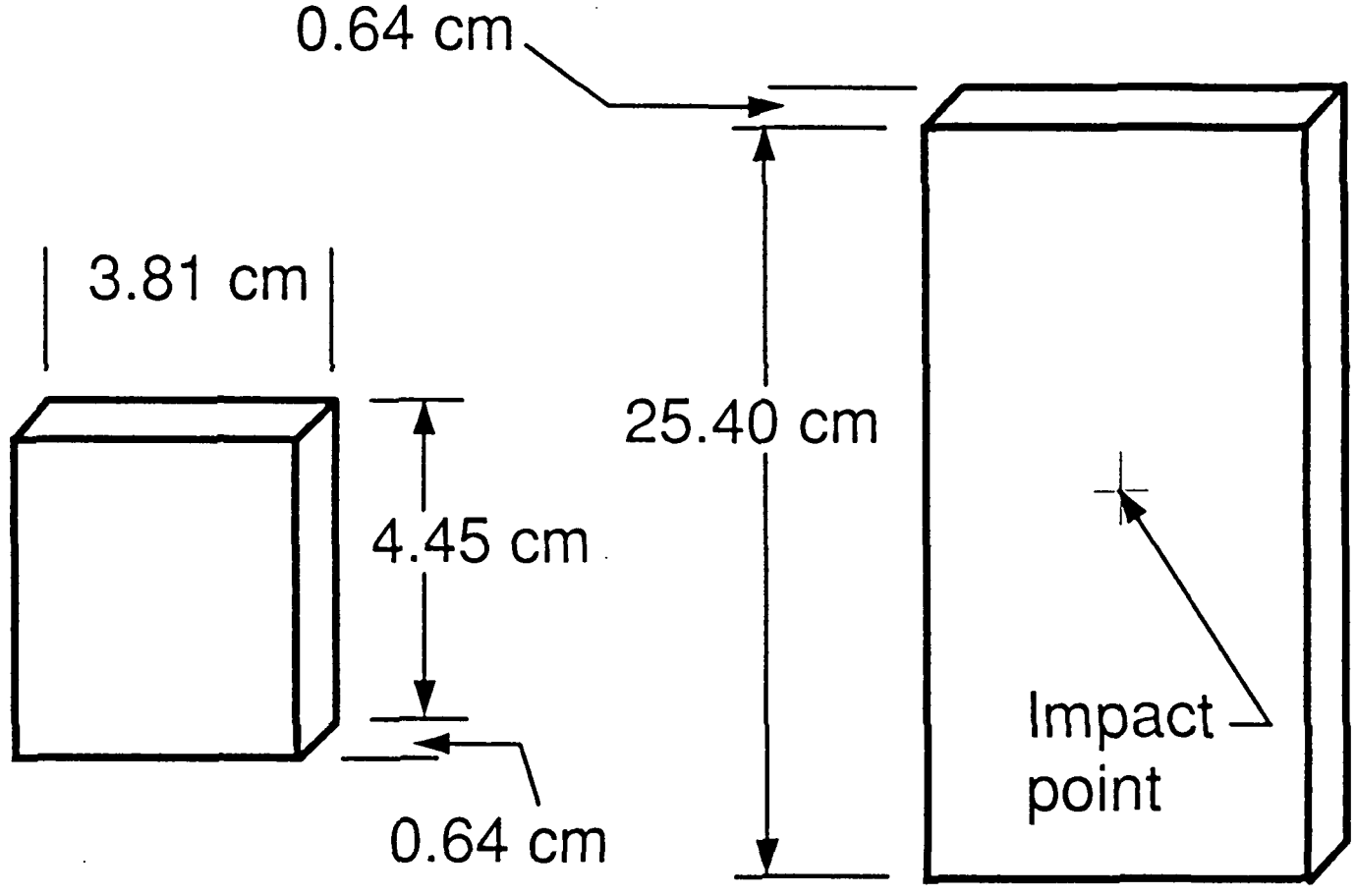

Short-block-compression specimen

Compression-after-impact specimen

Figure 3. Typical "dumbbell" shape of interlaminar damage.

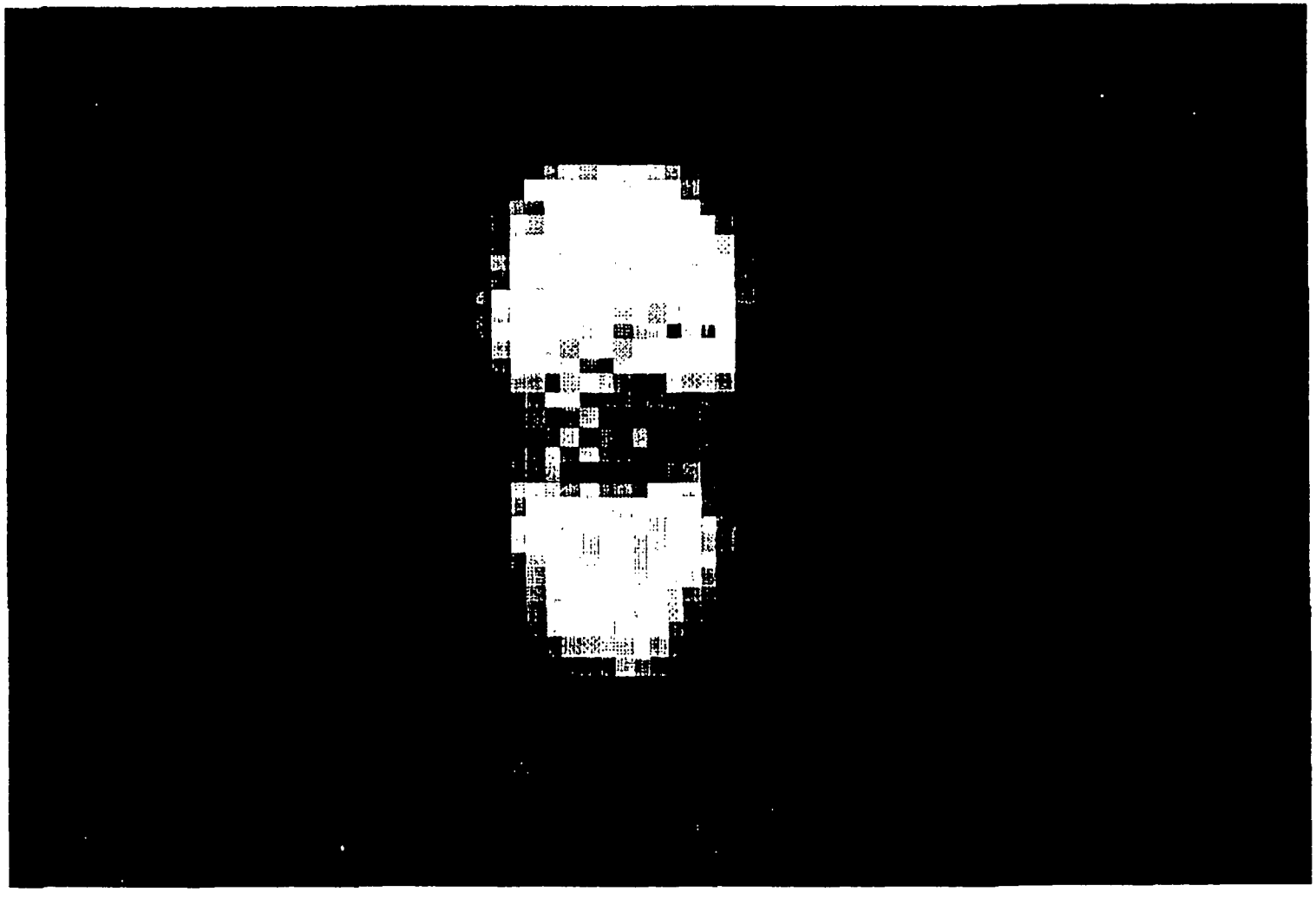

Figure 4. Compression strength of [0/90] composite materials.

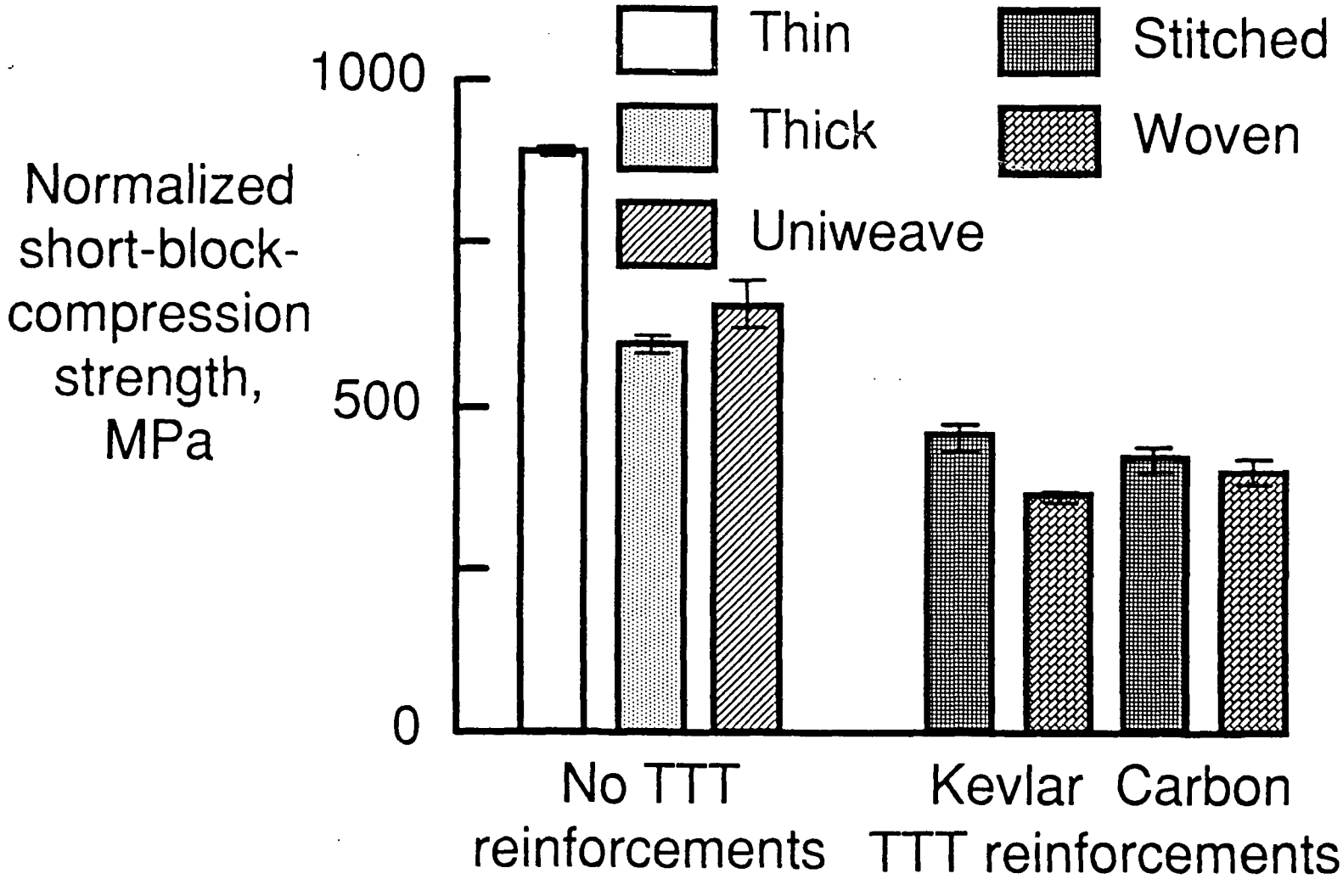

Thin - $[(0/90)_2/0/(0/90)_5/0/(0/90)_3/0]_S$

Thick - $[(0_5/90_5)_2/0_3]_S$

Uniweave - [0/90/0/90/0/90/0/90/0]

All strengths are normalized to 60 percent fiber volume fraction.

Figure 5. Failure modes of short-block-compression specimens.

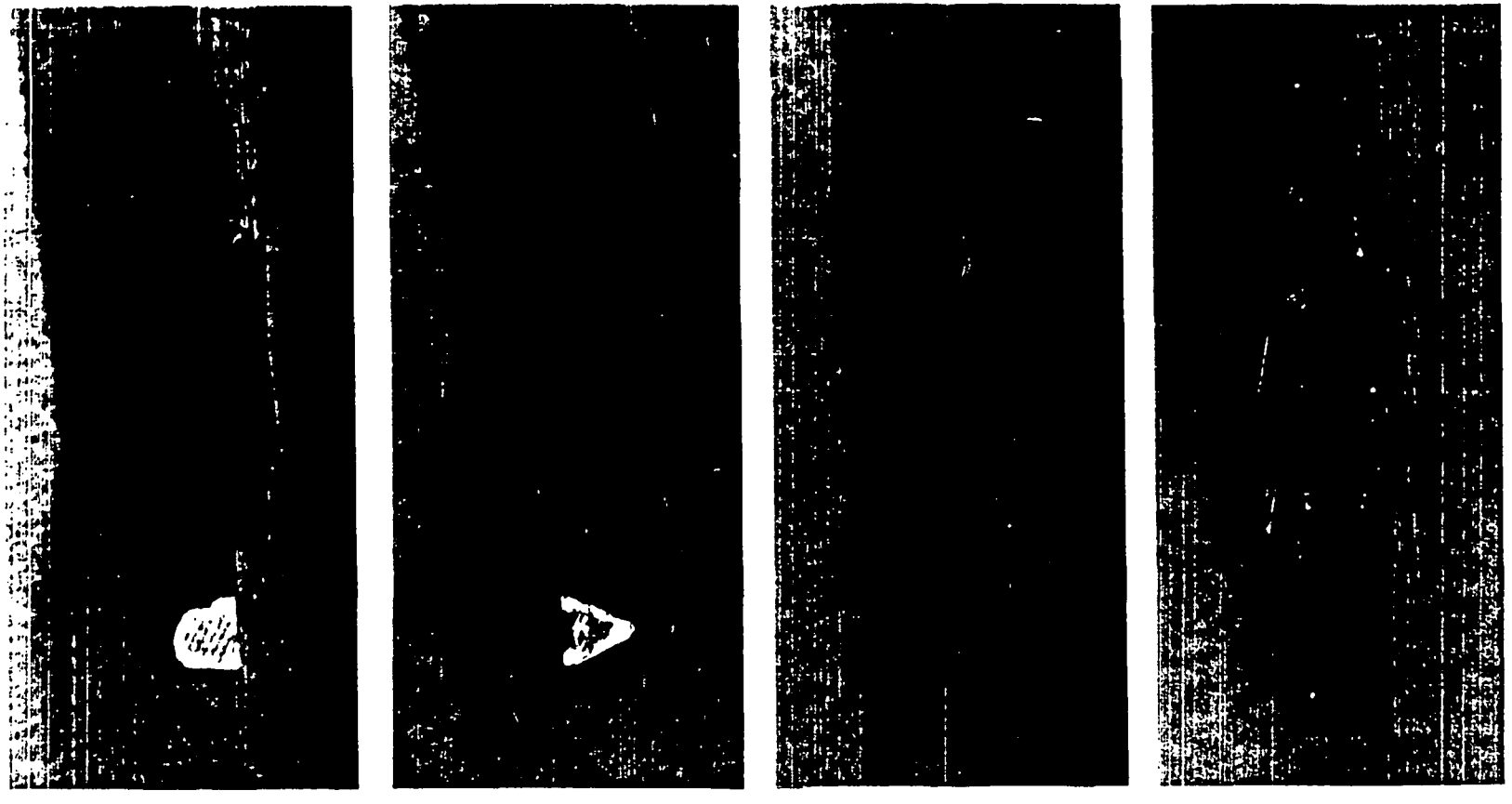

Figure 6. Photomicrographs of stitched and integrally woven composite material.

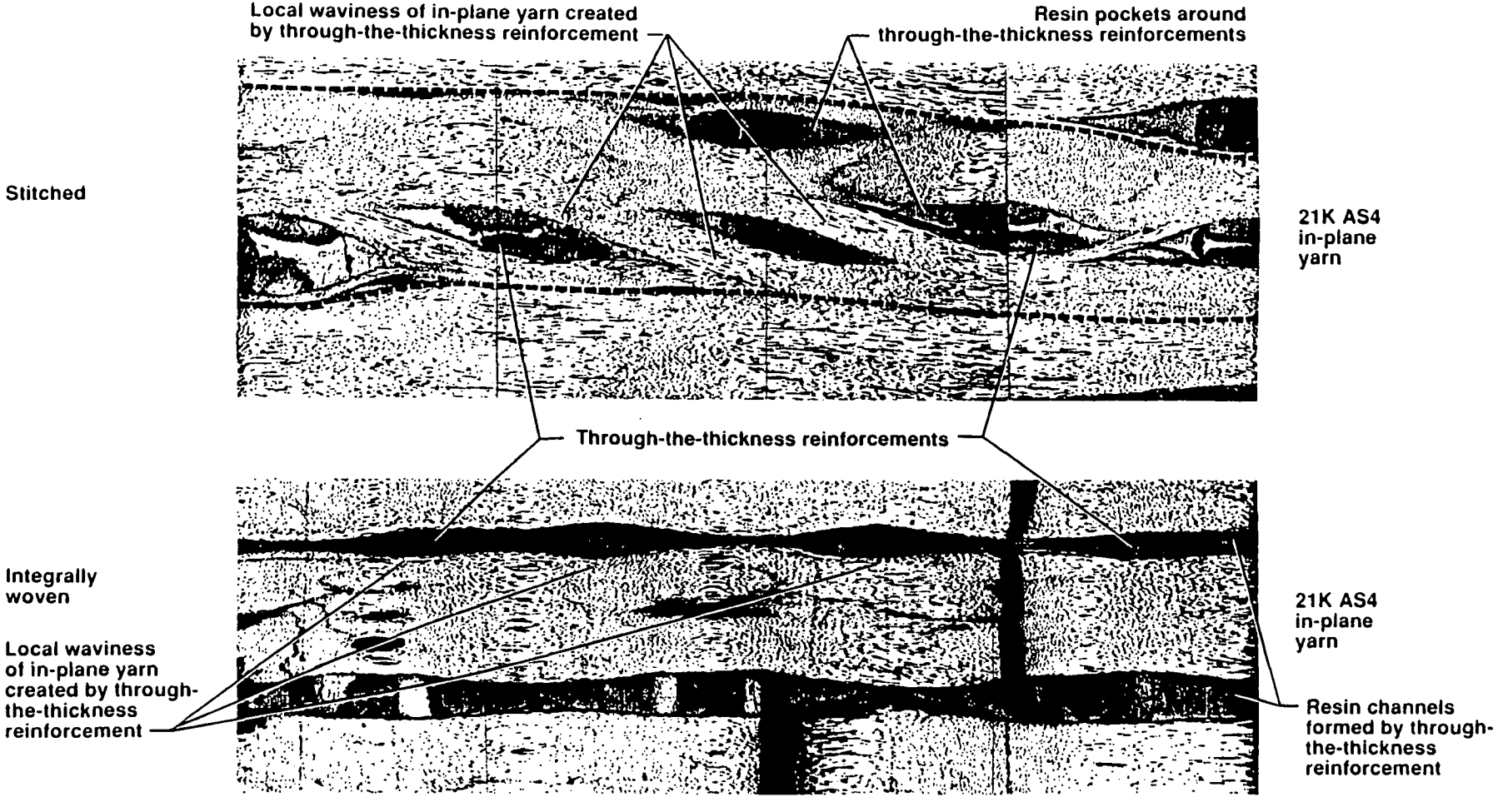

Figure 7. Photomicrographs showing reduced resin in yarn bundle.

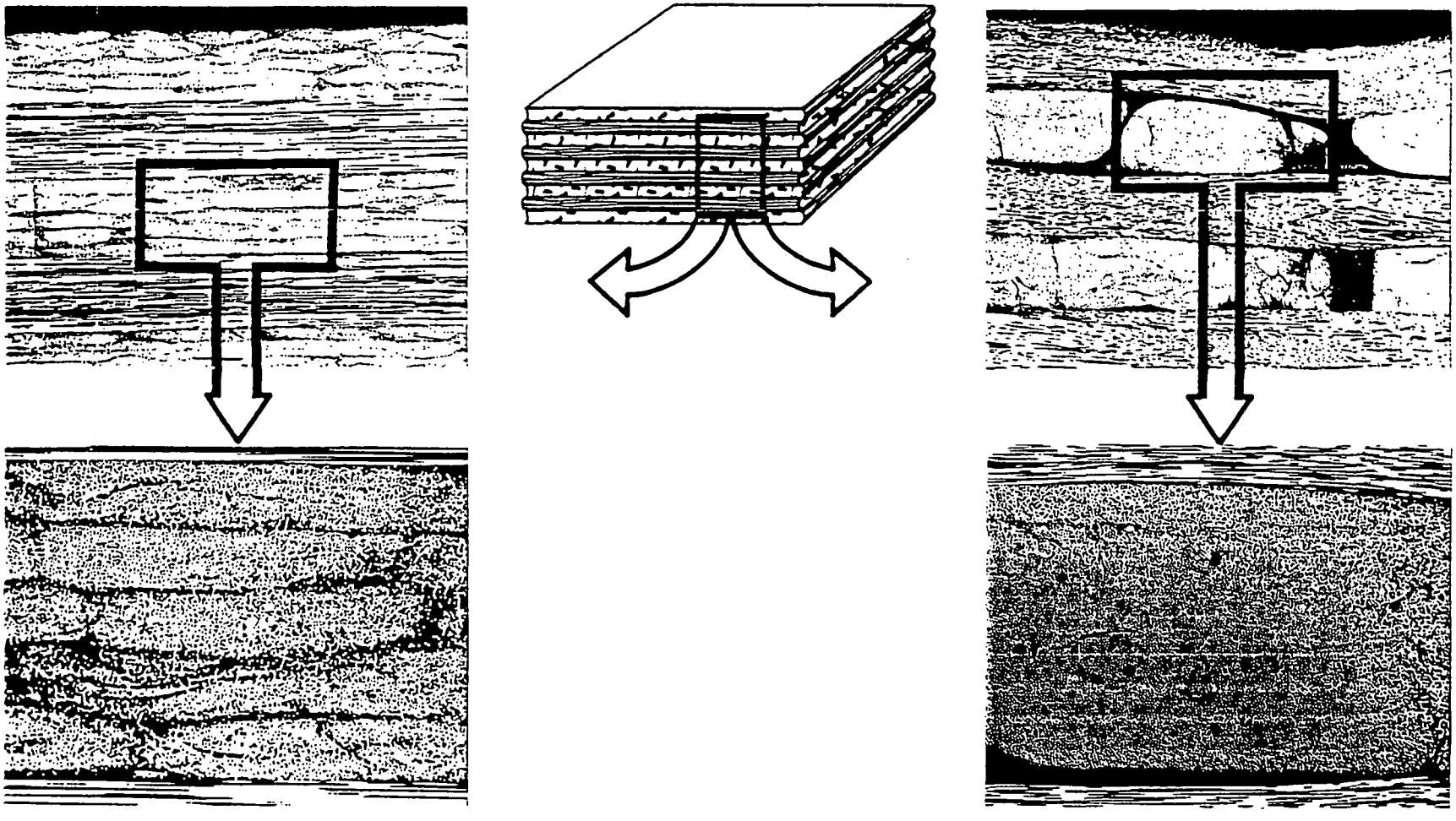

"Thick" tape

Kevlar stitch

Figure 8. Drop-weight-induced damage.

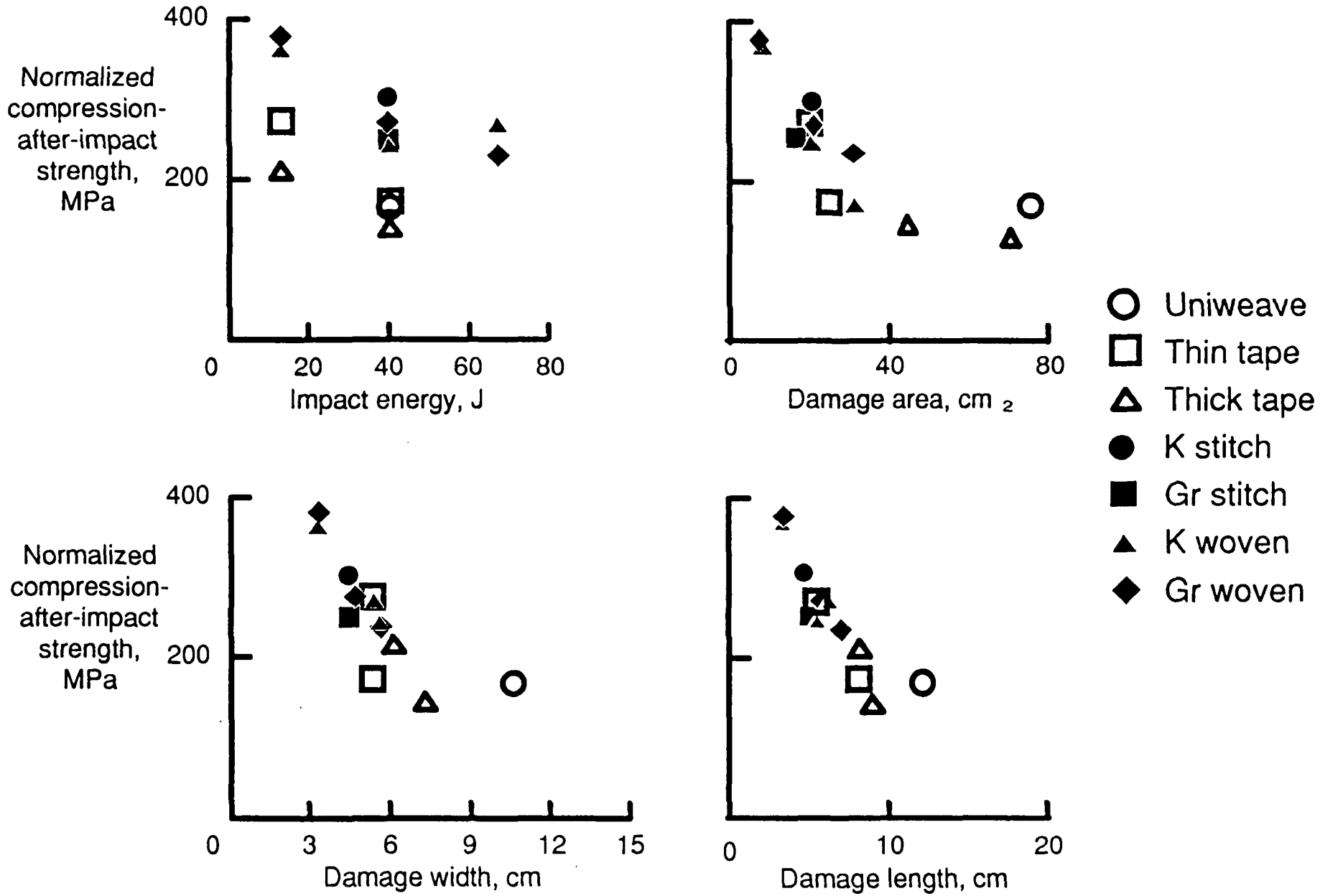

All strengths normalized to 60 percent fiber volume fraction

Figure 9. Air-gun-induced damage.

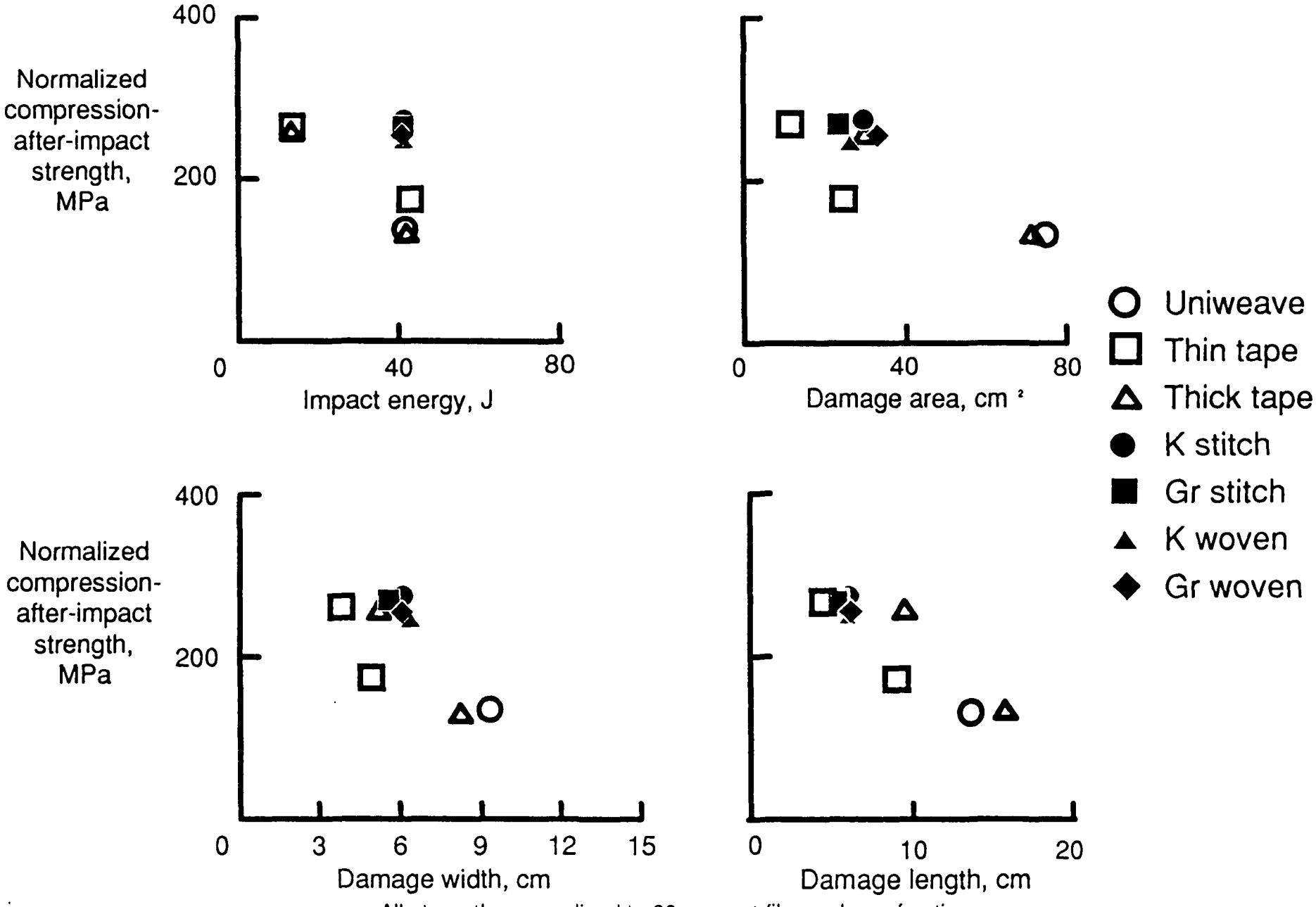

All strengths normalized to 60 percent fiber volume fraction

Figure 10. Failure modes of compression-after-impact specimens.

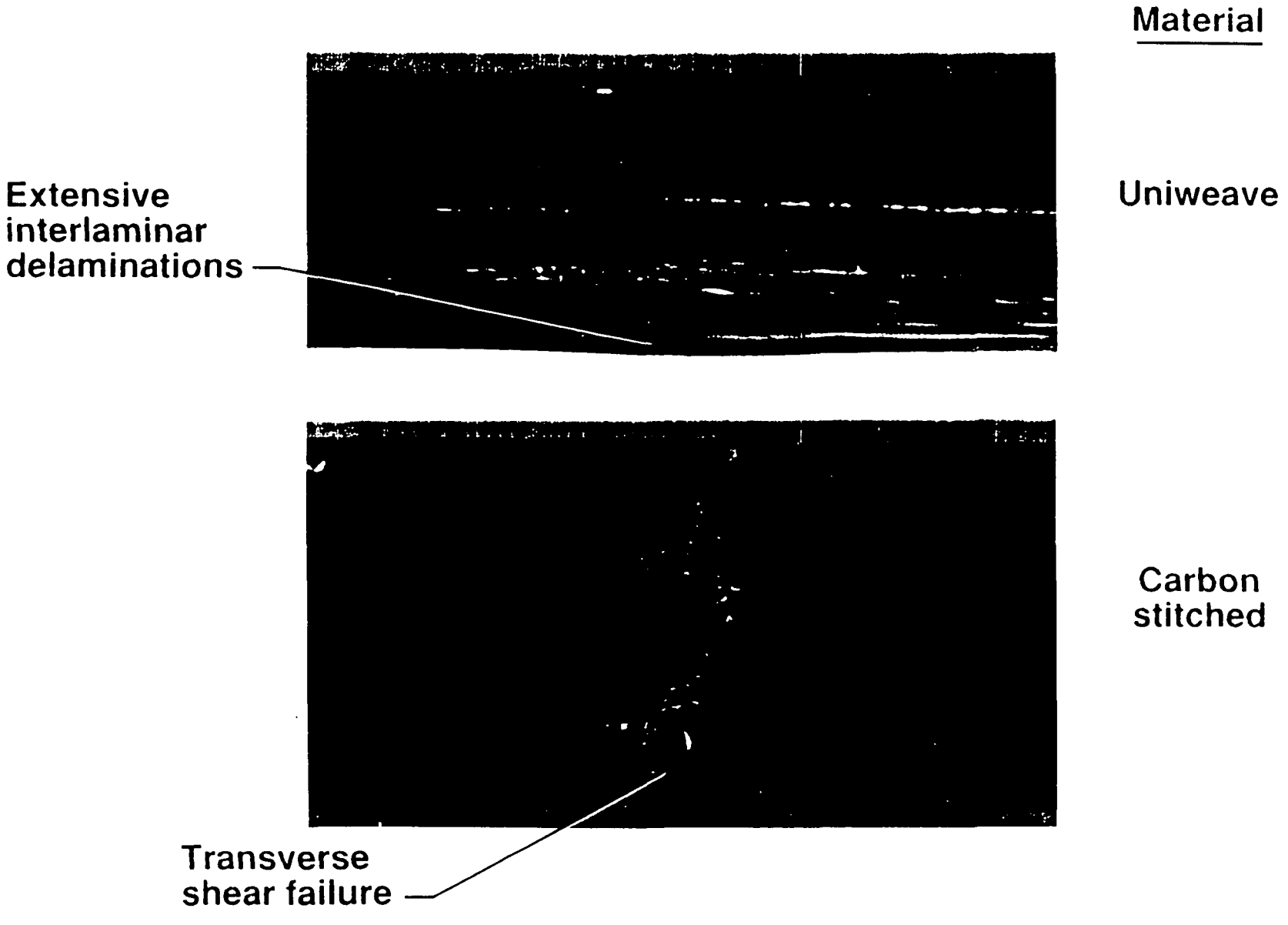

Figure 11. Influence of impact method and energy on damage.

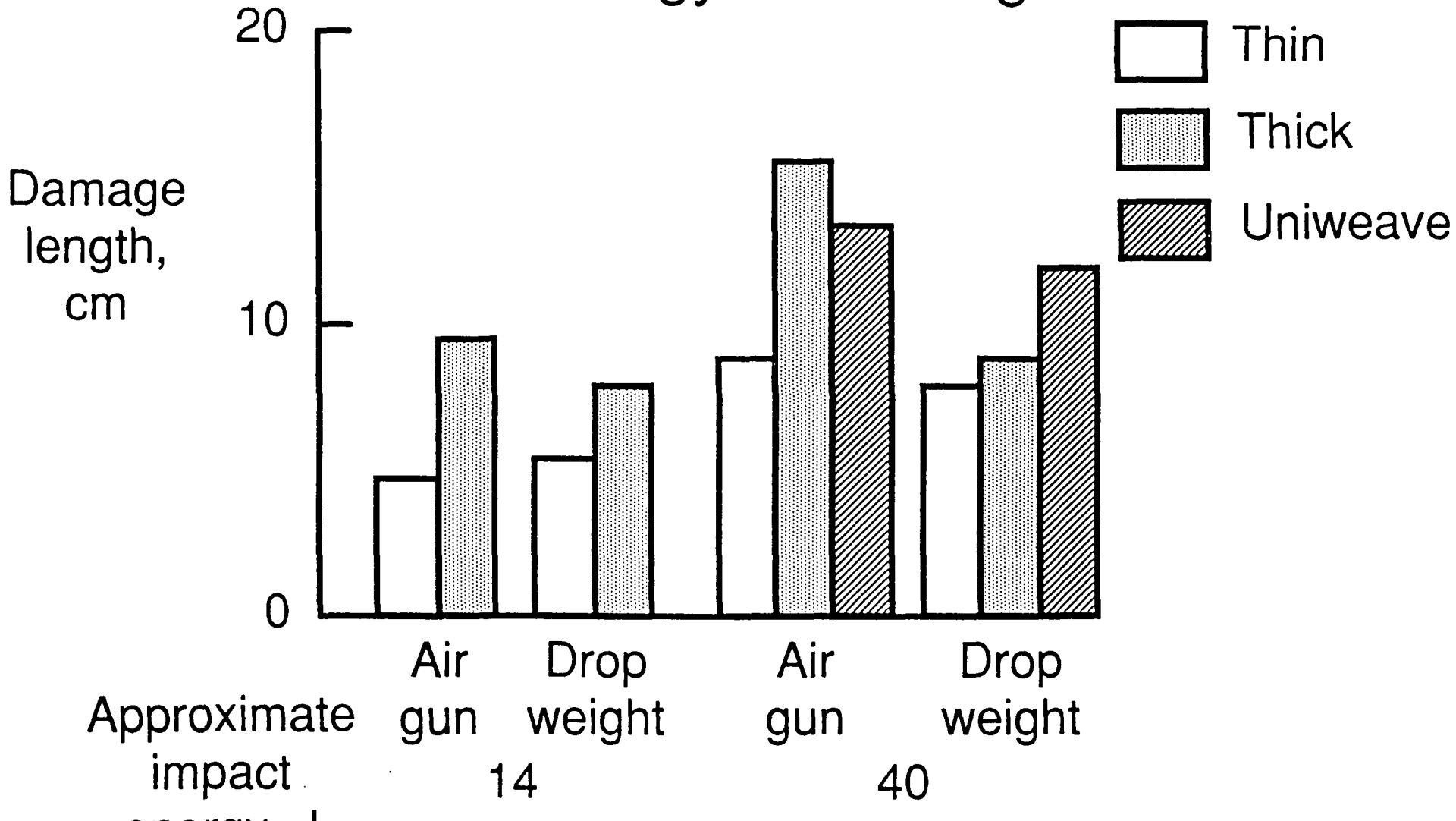

Thin - $[(0/90)_2/0/(0/90)_5/0/(0/90)_3/0]_S$

Thick - $[(0_5/90_5)_2/0_3]_S$

Uniweave - [0/90/0/90/0/90/0/90/0]

Figure 12. Influence of impact method and reinforcement on damage length.

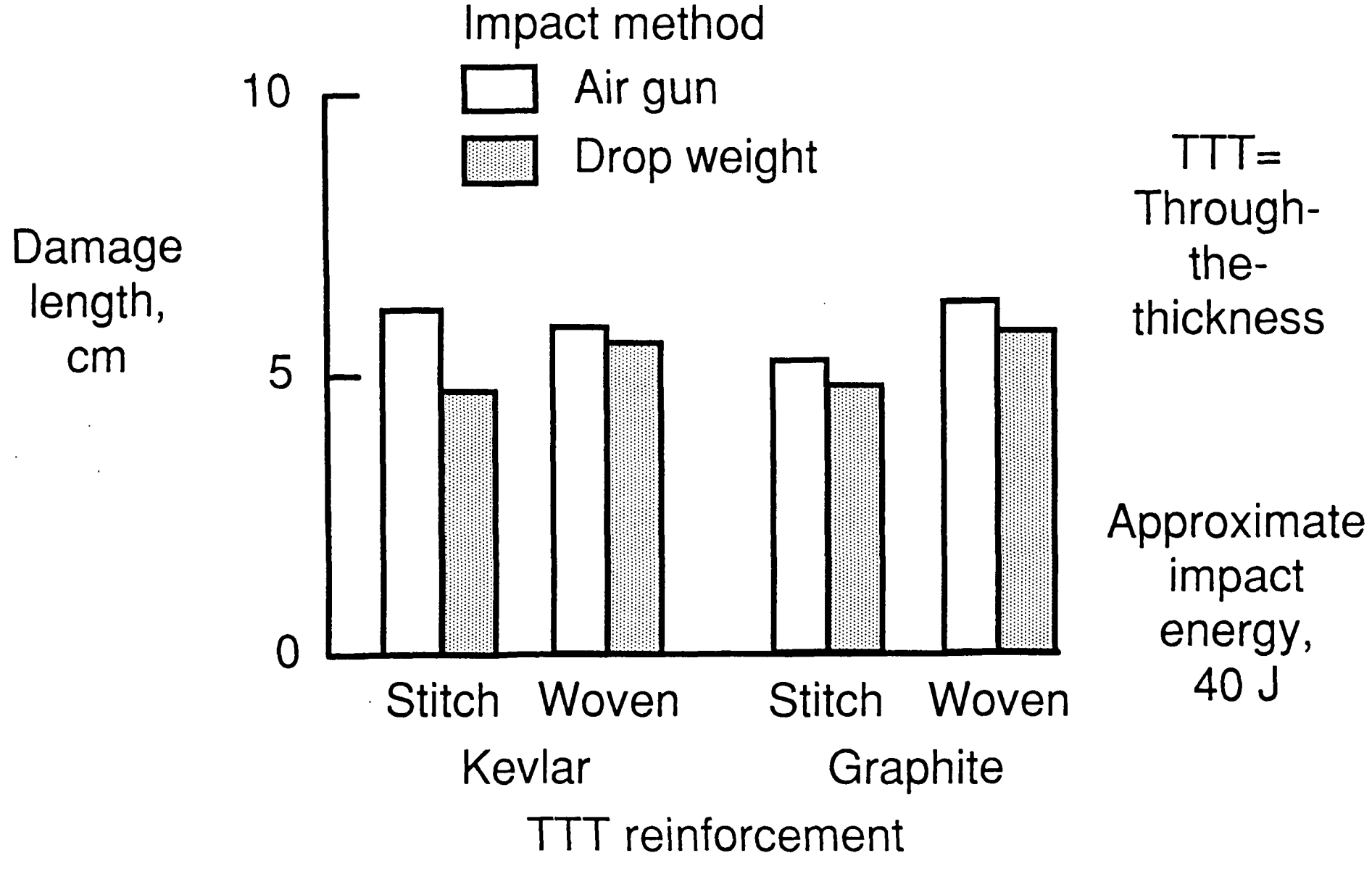

Figure 13. Influence of impact method and energy on CAI strength.

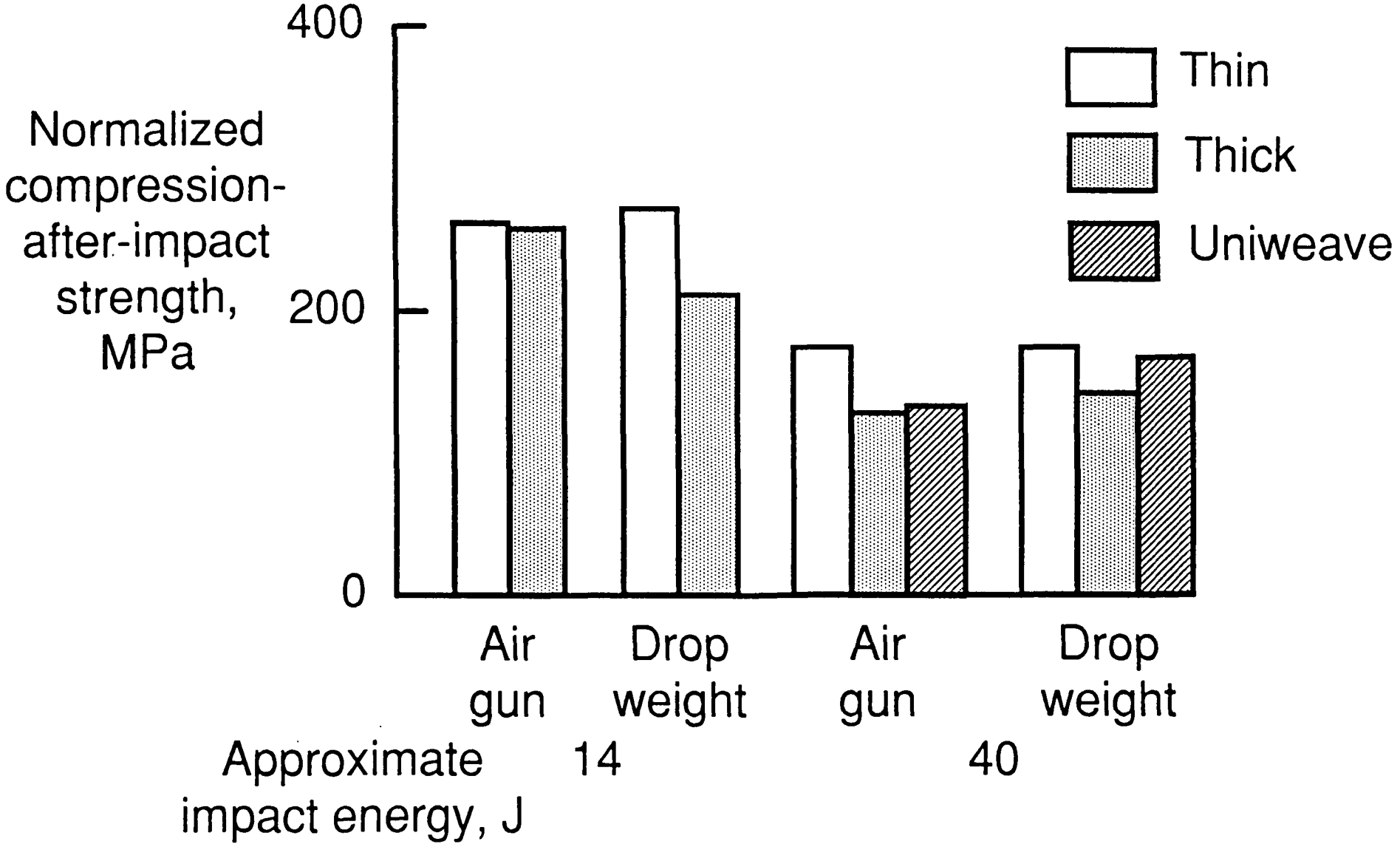

All strengths normalized to 60 percent fiber volume fraction

Figure 14. Influence of impact method and TTT reinforcement on CAI strength.

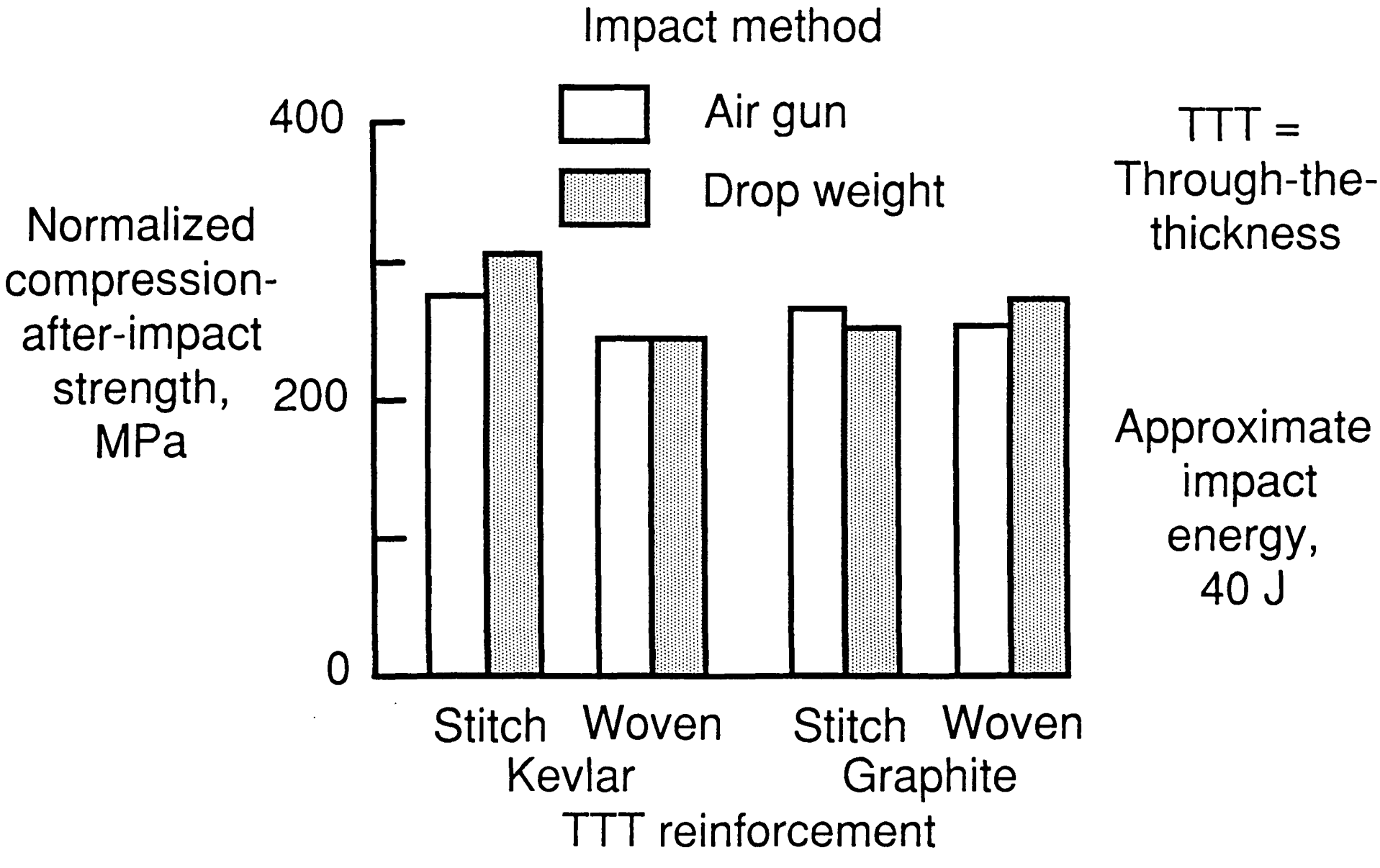

All strengths normalized to 60 percent fiber volume fraction

Figure 15. CAI strength of drop-weight-impacted specimens.

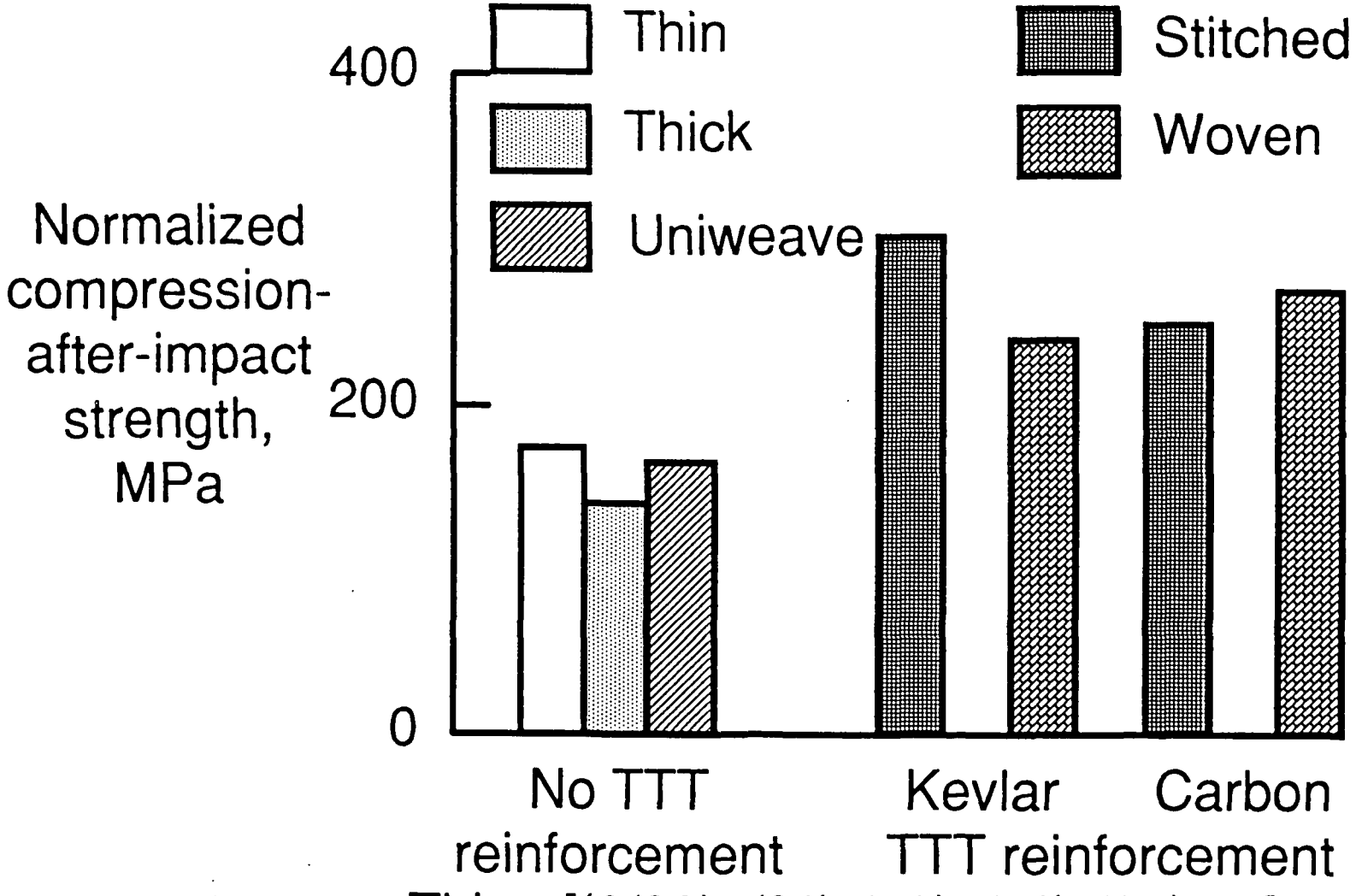

Approximate impact energy, 40 J

Thin - $[(0/90)_2/0/(0/90)_5/0/(0/90)_3/0]_S$

Thick - $[(0_5/90_5)_2/0_3]_S$

Uniweave - [0/90/0/90/0/90/0/90/0]

All strengths normalized to 60 percent fiber volume fraction

Figure 16. CAI strength of air-gun-impacted specimens.

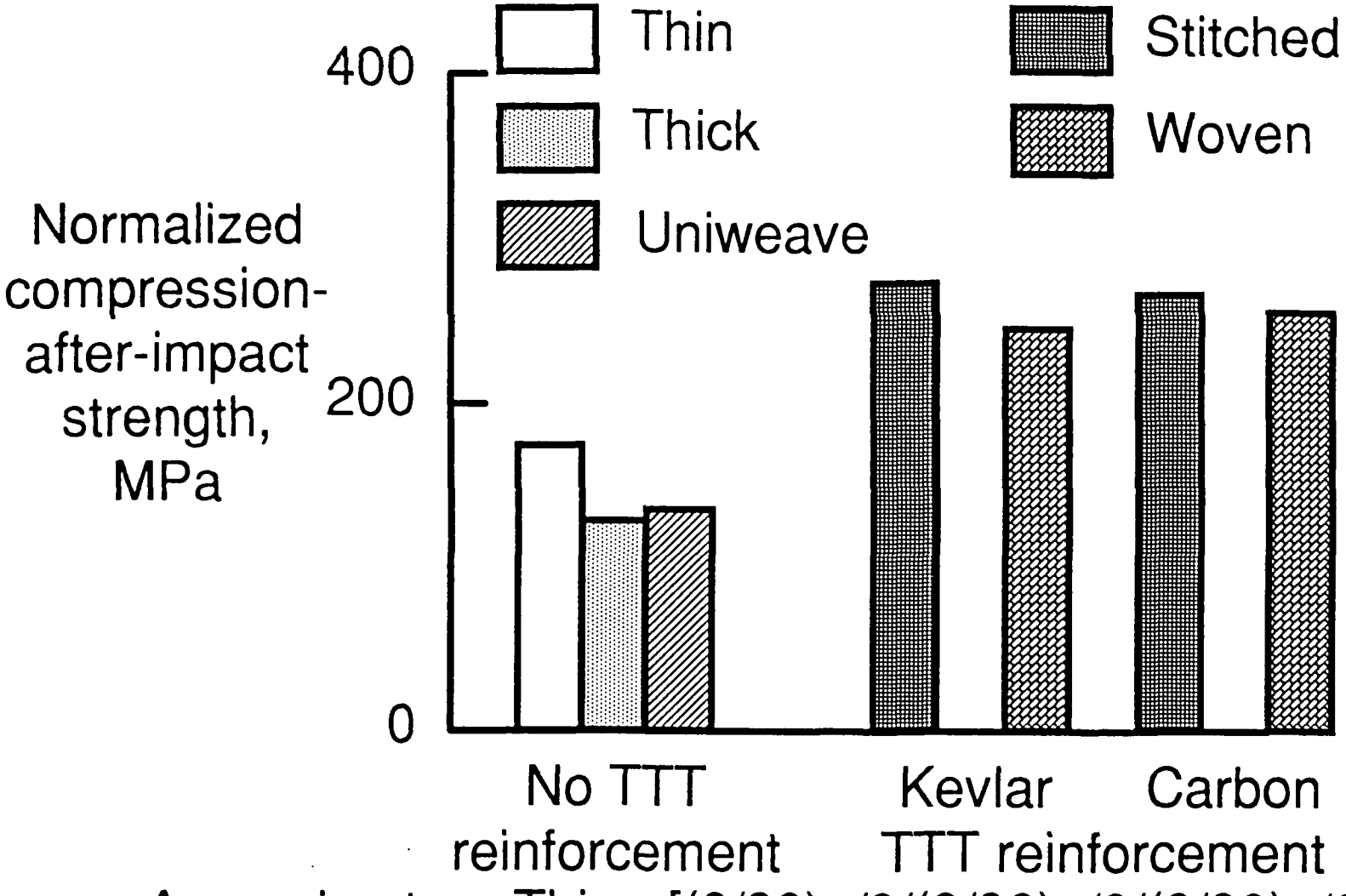

Approximate impact energy, 40 J

Thin - $[(0/90)_2/0/(0/90)_5/0/(0/90)_3/0]_S$

Thick - $[(0_5/90_5)_2/0_3]_S$

Uniweave - [0/90/0/90/0/90/0/90/0]

All strengths normalized to 60 percent fiber volume fraction

Figure 17. Typical B-scans of impacted panels.